ABSTRACT

Title of Thesis: MACHINE LEARNING ASSISTED DESIGN OF MXENE AEROGELS FOR PERSONAL THERMAL MANAGEMENT

Meera Kesavan, Master of Science, 2023

Thesis Directed By: Dr. Po-Yen Chen, Department of Chemical and Biomolecular Engineering

Personal thermal management is necessary in maintaining body temperature in humans through the use of building insulation, personal garments, and heating or cooling units. Electrically conductive aerogels can be used as a multifunctional material, where the aerogel structure is intrinsically thermally insulating, and the incorporation of electrically conductive components allows for Joule heating of these materials for wearable heaters. $Ti_3C_2T_x$ (MXene) has been incorporated in materials for Joule heating due to its excellent electrical conductivity. Cellulose and gelatin based aerogels have been used as bio-based materials with good structural properties in aerogels. Due to the large range of possibilities in parameters for aerogel formation, from percentage of components in each sample to sample concentration and presence or absence of glutaraldehyde, it can be tedious to test a matrix of recipes and determine the effects of each component on the electrical properties. To assist in the design of highly conductive aerogels machine learning was used as it uses a data-driven approach to analyze the effect of inputs, sample composition in this case, to predict a set of inputs that will return a desired output, which is a highly conductive aerogel.

Aerogels of various compositions were fabricated and their resistances and sensitivities to applied pressure were measured to screen for highly conductive recipes and for strain insensitive samples. Of these samples, a strain insensitive sample recipe and a strain sensitive sample recipe were selected for Joule heating tests. Low voltages of 2 Volts and below, were applied to the aerogel samples and the temperature increase was measured. The stability of these samples under multiple heating and cooling cycles were tested both with and without applied compression. Through these tests we determined a strain

insensitive aerogel recipe for stable temperature control regardless of pressure applied. This aerogel recipe was found to have a thermal conductivity comparable to common insulating materials at a much lower density. A machine learning model was then trained from the aerogel compositions and measured resistance values, and a prediction model with a low mean relative error of 19% was developed to assist in conductive aerogel recipe formulation.

MACHINE LEARNING ASSISTED DESIGN OF MXENE AEROGELS FOR PERSONAL THERMAL MANAGEMENT

by

Meera Kesavan

Thesis submitted to the Faculty of the Graduate School of the
University of Maryland, College Park, in partial fulfillment
of the requirements for the degree of
Master of Science
2023

Advisory Committee:
Prof. Po-Yen Chen, Chair
Prof. Akua Asa-Awuku
Prof. Nam Sun Wang
Prof. Chen Zhang

Dedication

This thesis is dedicated to my family.

Acknowledgements

I would like to thank my advisor for his guidance throughout this whole process. I would also like to thank my lab mates for their mentorship and assistance.

Table of Contents

List of Figures

1: Introduction

1.1: Aerogels: What are they? What are they made from? How are they made?

1.1.1: What are aerogels?

The concept of aerogels was first introduced in 1932 by Kistler, who was interested in preserving the network structure of gels by removing the liquid with minimal shrinkage by using supercritical drying (1). Kistler formed aerogels out of silica, alumina, nickel tartrate, oxides such as stannic oxide and tungstic oxide, and organic materials including gelatin, agar, nitrocellulose, and egg albumin. Following this research, many aerogels have been made using sol-gel chemistry and supercritical drying; however, materials dried under other methods such as freeze-drying have also been called aerogels. The term aerogel has been used to refer to networked or porous materials with a relative pore volume of approximately 90% or higher (2). These are dry gels where the liquid has been completely replaced by gas or air without collapsing the structure.

1.1.2: What are aerogels made from?

Aerogel materials and precursors can be divided into two groups: organic and inorganic. Inorganic gels include metallic salts and oxides as well as silica and water glass. Organic gels include low molecular weight gelators, biopolymers, and lignocellulosic biomasses (3). Inorganic aerogels can be further divided into oxide and carbide aerogels while organic aerogels can include graphene, carbon nanotube, and carbon aerogels (4). Carbon aerogels can be made of different formaldehyde molecules and have a very high thermal stability, maintaining its porous network at high temperatures up to 2800 (4).

1.1.3: Aerogel formation methods.

Aerogels are typically produced through the same process: gel formation, solvent exchange, and drying with optional functionalizing or coating afterwards. Initial silica aerogels were formed through the sol-gel technique, where precursors go through hydrolysis and condensation reactions to form a network in liquid solvent (5). To produce the aerogel, the gel must be dried to remove the solvent but leave the solid network intact, and this can be done through supercritical drying, evaporative drying in ambient or vacuum pressure conditions, and freeze-drying where the solvent is frozen and sublimated in vacuum conditions (Figure 1a) (5).

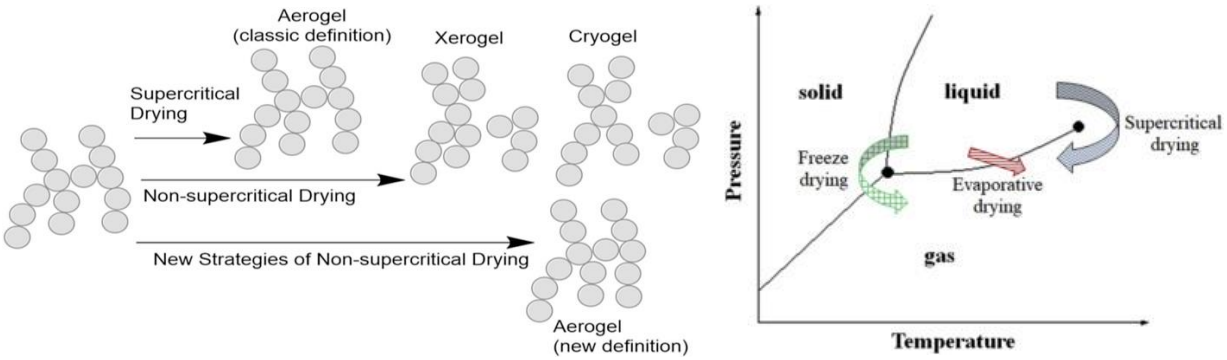

Figure 1: a) Methods to dry gels to form aerogels, b) the phase diagram showing how each drying method transitions from liquid to gas *(5)*.

There are a few different ways to transition the solvent from the liquid to the gas phase without damaging the solid network in the gel. As seen in Figure 1b, freeze-drying avoids the solvent triple point, evaporative drying goes through the liquid-gas equilibrium line, and supercritical drying bypasses the liquid-gas equilibrium line (Vareda, 2018). With this variety in aerogel precursors and formation methods, it is then possible to formulate specific and targeted materials with properties of interest for applications ranging from protein and small molecule delivery to thermal or acoustic insulation.

1.2: Applications for Aerogels

Since aerogels can be made of a variety of materials and can be formed from different solvent exchange methods, the thermal conductivity, electrical conductivity, surface area, and pore size can be tailored according to the application or need. Due to their high porosity and many gas-solid boundaries, silica aerogels can be used for acoustic insulation, optical applications, and thermal insulation (6). Also due to their porosity, ions can be intercalated into aerogel networks for batteries and capacitor electrodes (6).

As the variety of methods and materials used in producing aerogels have increased, the applications for aerogels have also expanded to include use in biomaterials. Aerogels have been used as drug carriers via silica and bio-based aerogels, as scaffolds for bone-growth in tissue engineering, as potential materials for medical implantable devices such as artificial heart valves, as acoustic absorption materials for biomedical imaging through sound impedance differences seen in ultrasound imaging, and as matrixes for biosensors (7). These materials can also be used in further life science applications through the encapsulation of enzymes and other biomaterials, the encapsulation of chemicals used in agriculture such as herbicides and fertilizer, and bio-based food packaging materials for temperature control and moisture absorption (7).

1.3: Strategies for Personal Thermal Management

1.3.1: Thermal Conductivity in Aerogels

Thermal conductivity consists of the gas, solid, convective, and radiative components

$$\lambda = \lambda_s + \lambda_g + \lambda_c + \lambda_r$$

where λ_s is the thermal conductivity of the solid phase, λ_g is the thermal conductivity of the gas phase, λ_c is the convective thermal conductivity, and λ_r is the radiative thermal conductivity (8).

λ_s is the heat transfer in the network structure of the aerogel, and this is usually affected by density. The thermal conductivity can be further simplified by the following assumptions. λ_c is negligible in mesoporous and microporous materials, where the pores are smaller than 1 mm. λ_r can be ignored for porous materials close to room temperature (8).

In general, the thermal conductivity of the solid phase can be reduced by reducing the bulk density of the aerogel, and the thermal conductivity of the gas phase can be reduced with narrower pore sizes (9). The thermal properties of materials are a function of that material's thickness, density, temperature, and moisture content. The more cellular an insulating material is, and the smaller cells exist, the more thermally resistive the material will be since there will be less air moving, and this can be done by increasing the density of the material (10). However, as mentioned before, increasing the bulk density of an aerogel will increase thermal conductivity of the solid phase, so there will be a trade-off between smaller pore sizes and bulk density of insulating materials that may be different for each insulation system.

1.3.2: Thermal Conductivity of Common Insulators

Similar to aerogel classification, insulating materials can be grouped into inorganic, organic, combination, and advanced materials, and can come in various form factors depending on their intended application from porous to rigid foams. Porous materials have thermal conductivities between 0.02 to 0.08 W/mK, while fibrous insulation materials have thermal conductivities between 0.04 to 0.09 W/mK but suffer from moisture absorption that would increase thermal conductivity (11). Anh et. al. found that in closed-cell materials like foams, higher densities lead to lower thermal conductivities due to smaller pores and less total air, but in natural fiber materials, as density increases the thermal conductivity decreases to a minimum and

then increases as the density further increases due to heat conduction through the solid fibers (Figure 11).

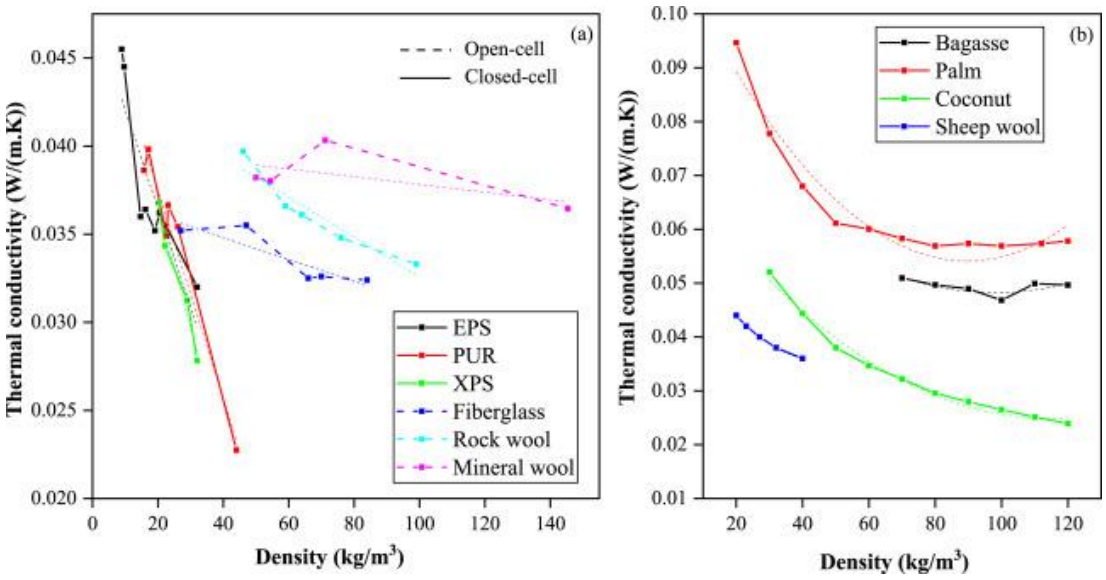

Figure 2: The effect of density on thermal conductivity for common insulating materials *(11)*.

1.4: Conductive Aerogels for Personal Thermal Management

1.4.1: Strategies for Personal Thermal Management

Personal thermal management is a method to direct a suitable thermal dose to an individual for their optimal thermal comfort. It generally is used to improve the health of outdoor athletes, firefighters, soldiers, law enforcement personnel, construction workers, and other personnel that may experience significantly cooler or warmer temperatures in their day-to-day life or employment. It can also be used in health care for specific temperature control for people with fever, chills, wounds, neurologic disorder, or other ailments or statuses that may cause difficulty in regulating body temperature.

A form of personal thermal management is a personal-heating garment, where the heating element can be either electrical or chemical. For electrical-heating elements, the element is

generally embedded inside the cloths to generate heat for human skin; these elements can be electrical wires, electrically conductive rubbers, polymers, and fabrics (12). For chemical heating elements or garments, the garment uses chemical heating as substitute for electrical heating inside the cloths. However, there are limitations: the chemical reaction that generates the heat should be safe for human skin, where the temperature is less than 42 degrees C, and the garment should be sealed or protected to prevent chemical leakage (12).

1.4.2: Aerogels for Personal Thermal Management

Aerogels are good materials and structures for wearable heaters due to their 3D networked inner structure, which provides micro channels to allow effective air transmission to the skin, and due to their low thermal conductivity from the porous structure, which inhibits loss of thermal energy and reduces human energy consumption. The usual metrics that are measured for these aerogels are breathability for describing the air permeability in the material, measured in g/cm^2*d, and electrical conductivity to describe how well the material can be used as an electric heater, measured in S/m (13). The water contact angle of aerogels is also measured for applications requiring hydrophobic aerogels, where higher angles mean better hydrophobicity (13). In thermal management, the thermal conductivity is the most studied metric as it allows for comparison between new materials and existing commercial materials.

1.4.3: Understanding Joule Heating

Electrically conductive materials can be used as electric heaters for wearable personal thermal management. This can be achieved through Joule heating, where a voltage is applied to a resistor, and due to non-ideal heating excess energy is lost as heat in the material. The heat generated follows Joule's law, shown below.

$$Q = \frac{U^2}{R * t}$$

Q is the heat generated, U is the voltage applied, R is the resistance of the aerogel, and t is the time. The heat produced is inversely proportional to the resistance of the material and the temperature is linearly proportional to the voltage squared (14). As the resistance of a material increases, more voltage is required to reach the same temperature compared to a lower resistance material. Electrically conductive aerogels can serve as the resistors for Joule heating, where it is necessary to have low resistance materials for heating for electrical safety for human centered uses.

1.4.4: Joule Heating in Aerogels for Wearable Heaters

Aerogels are attractive three dimensional structures for thermal insulation, and incorporation of electrically conductive materials into the structure allows for Joule heating. Menzel et. al investigated the effects of Joule heating in ultra-light three dimensional graphene aerogel assemblies with densities of 10 mg/mL (15). They observed a quadratic correlation of input voltage with temperature and a linear relationship of the electrical power input with temperature, showing that their aerogels followed Joule's law. The heating profile of these materials included an initial heating regime where the temperature rapidly increases and a slower heating regime that was likely controlled by the conductive and convective heat losses in the material (15). The group then conducted voltage cycling measurements and showed that their nanocarbon aerogels were suitable for applications with rapid heating and cooling with minimal hysteresis (15). Electrically conductive aerogels are a promising material for wearable heaters, but there needs to be more investigation into how incorporation of electrically conductive materials may affect the thermal insulating properties of the structure.

1.4.5: Piezoresistivity of Conductive Aerogels

The addition of conductive materials to a three dimensional network such as an aerogel introduces the possibility of the resistance of the material changing as a force is applied, also known as piezoresistance. Conductive three-dimensional networks have been used as piezoresistive pressure sensors, transducing pressure changes into electrical signals, in this case resistance, and aerogels specifically have been used for pressure sensors due to their large deformation space and ability to withstand high pressures (16). Materials such as graphene have been used in piezoresistive sensors due to their high specific surface area and the resistances of nanocomposites fabricated from graphene have been monitored under cyclic compression to determine if the resistance, and response of the pressure sensor, changes over multiple cycles of loading and unloading force (17). Unlike pressure sensors, materials needed for wearable heaters need to be highly pressure insensitive in order for their temperature to remain stable with and without compression.

1.5: Materials for Conductive Aerogels for Thermal Management

1.5.1: MXenes as a Promising Component for Conductive Aerogels

MXenes are conductive materials formed from layered two-dimensional transition metal carbides or nitrides with a general formula of $M_{n+1}X_nT_x$. M is an early transition metal, X is carbon or nitrogen, T is the surface termination unit, usually oxygen, fluorine, or a hydroxyl group, and n is 1, 2, or 3, which denotes how many layers are in the structure. They are formed from selective etching of the "A" elements from the parent "MAX" material with a formula of $M_{n+1}AX_n$, where M, X, and n are the same as those for MXene, and A is elements from groups 13 and 14 on the periodic table (18).

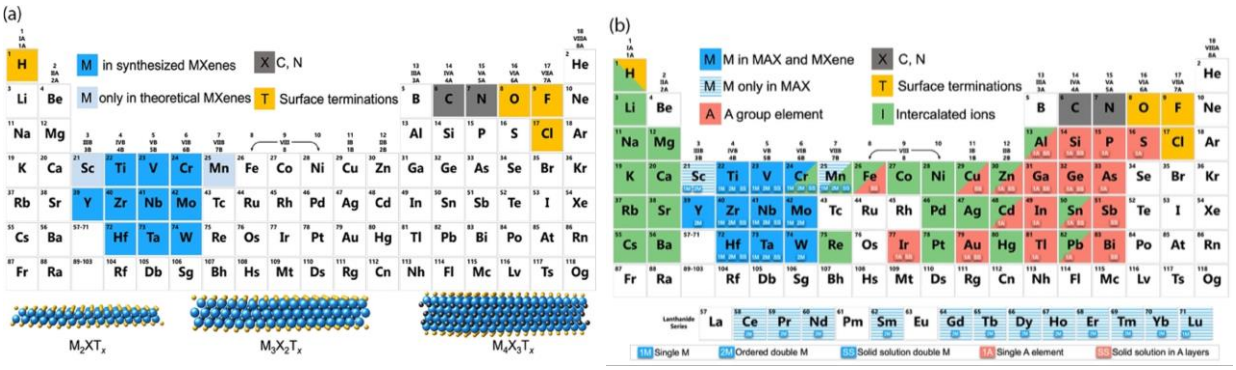

Figure 3: a) Common elements found in MXenes. Elements in blue are the early transition metals "M", elements in gray are either carbon or nitrogen, and elements in yellow are the surface termination groups, b) Common elements found in both the MXene precursor "MAX" and MXene, where the additional shaded elements represent the elements "A" that are etched from the MAX phase (in red) and the intercalating ions (in green) *(18)*.

Not only can MXenes be multi-layered, they can also be composed of more than one type of transition metal, as seen in Figure 4.

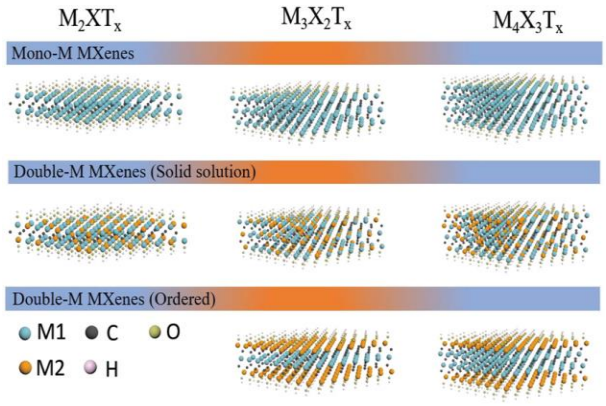

Figure 4: Structure of MXenes with one, two, and three layers displayed in each column for single and double metal MXenes displayed in the rows *(19)*.

Due to their excellent electrical conductivity, flexible surface terminal groups, and interesting layered structure, MXenes have been used in a variety of applications. MXenes have also been used for catalytic reactions such as the hydrogen evolution reaction, oxygen evolution reaction, oxygen reduction reaction, nitrogen reduction reaction, CO_2 electroreduction reaction, H_2 production, and for many heterogeneous reactions (19). Many various forms of MXenes have been synthesized; however, most research is conducted on $Ti_3C_2T_x$, which is the first discovered

MXene (18). The choice of MXene or MAX starting material, and the type of surface termination can influence the selectivity and reactivity of MXene (19). MXene based aerogels are also prevalent in literature and can be organized into all-MXene aerogels, MXene/carbon aerogels, MXene/polymer aerogels, and MXene/metal ion aerogels (20).

1.5.2: Cellulose Nanofibers as Aerogel Components

Cellulose is a promising material for aerogels, as it is an abundant natural polymer, is biodegradable, and is inexpensive. Cellulose has been traditionally used in applications such as paper, fabric, and building materials, but with new technological advances cellulose-based nanostructures have been fabricated. These include cellulose films, fibers, hydrogels, composites, and aerogels, where cellulose based aerogels have been used in adsorption, separation, insulation, biomedical materials, and supports for metal particles (21). Cellulose aerogels have comparable specific surface area, porosity, and density to silica aerogels, but they have a higher compressive strength (21). The increased compressive strength can be attributed to the strong hydrogen bonds between the molecular cellulose chains from the many hydroxyl groups (22). To improve the gelation behavior of nanocellulose and improve the overall strength of cellulose aerogels, a chemical crosslinker such as glutaraldehyde or citric acid can be added to form covalent bonds between cellulose strands (22). Cellulose can be used in combination with other fillers or components to provide structural support while allowing for other material properties to be incorporated into the overall material.

1.5.3: Gelatin for Aerogels

To improve the structural formation of aerogels, gelatin was selected as a material for these electrically conductive aerogels. Gelatin is a bio-based material commonly found in skin, tendons, and bone and it is an attractive material due to its cost, biodegradability, and

biocompatibility. It has been used in the fabrication of soft aerogels for oil absorption due to its ability to form highly porous, elastic, and lightweight structures (23). Gelatin has also been used in combination with graphene oxide as aerogels for wound dressing, as the amine groups from the gelatin can form physical bonds with the oxygenated groups on graphene oxide (24). In MXene-gelatin composite aerogels, the gelatin served as a gelation agent, holding the MXene sheets together, to provide support on top of the van der Waals interactions holding the MXene nanosheets together (25). Gelatin will be used in combination with MXene, and cellulose nanofibers as the three major building blocks of the conductive aerogel recipes.

1.6: Machine Learning for Material Science

Machine learning is commonly attributed to computer science, communications, and control systems as it can be used to work with large amounts of data to create prediction models. Machine learning is defined as a part of the computer science field that allows computers to learn without direct programming by improving their performance at prediction or task completion through data fitting (26). Although machine learning can include statistical approaches, it focuses more on predictive ability of the model for large and complex datasets rather than hypothesis-based data analysis (26). Initial machine learning methods in the 1950s and 60s were focused on learning and pattern recognition systems, and these techniques have evolved to work with Big Data and use efficient data processing for optimization of a predictive machine learning model (27). Since it can quickly process large and complex data, machine learning can be used in fields from computer science, which was its initial use, to economics or biosciences.

Due to the large amounts of data that can be collected and that already is available, scientists are interested in quicker ways to predict or screen new materials for applications of interest. Machine learning starts with acquiring datasets or measuring data in the lab, and this

data is from material properties, images, chemical reactions, or literature (28). Features from the data are then extracted for their use as inputs to train a machine learning model, the model is trained using shallow or deep learning, and the model is finally validated to determine how accurate it is (28). Training and using a machine learning model has been used in material property analysis, discovering new materials, and quantum chemistry (28). As it is very versatile, machine learning can be used to determine optimal composition of an aerogel with electrical properties useful in personal thermal management.

2: Experimental Set-up

2.1: Aerogel Material Synthesis

Hydrochloric Acid (HCl, 37%) and Lithium Fluoride (LiF, powder, <100 μm, ≥99.8% trace metal basis), bleached kraft softwood pulp, 2,2,6,6-Tetramethylpiperidine 1-oxyl radical (Tempo 98%), sodium bromide (NaBr, >99.0%), sodium hypochlorite (NaClO), sodium hydroxide (NaOH), sodium carbonate (Na_2CO_3), and sodium bicarbonate ($NaHCO_3$) were purchased from Sigma Aldrich.

2.1.1: MXene Synthesis

Single layer Titanium Carbide (MXene) was synthesized as follows. 40 mL of 9M HCl was added to a 125 mL plastic beaker and kept stirring over an oil bath until the temperature of the liquid reached 35 C. 3.0 g of LiF was added to the beaker and the mixture was stirred until the LiF was dissolved completely in the HCl. 1.0 g of Titanium Aluminum Carbide was slowly added to the solution in intervals over the course of 5 to 7 minutes. The beaker was loosely covered with a cap to prevent H_2 gas from building up inside the beaker. The solution was stirred at speeds greater than 330 rpm and heated at 35 C for 24 hours.

After 24 hours, the MXene solution was removed from heat and allowed to return to room temperature before dividing the solution evenly into two 50 mL centrifuge tubes. Cold 2M HCl was added to each centrifuge tube until the total volume in each tube was approximately 45 mL. The solution was centrifuged at 8000 rpm for 5 minutes and the supernatant was disposed. The MXene was washed two more times with cold 2M HCl and then washed at least six more times with DI water until the pH of the supernatant liquid was between 5 and 6. During the wash steps, the centrifuge tubes were changed every three washes and the MXene suspension was

vortexed thoroughly to prevent MXene deposition on the bottom of the tube before each centrifugation. When necessary, the centrifugation speed was increased to 10,000 rpm and the time was increased to 20 minutes for the final washes.

After the final wash, a maximum of 35 mL of DI water was added to the MXene in the centrifuge tubes to target a concentration of at least 10 mg/mL and the suspension was thoroughly mixed. The suspension was sonicated in cold water for 1 hour to delaminate the MXene sheets. The suspension was then centrifuged at 3000 rpm for 30 minutes and the supernatant was collected and stored in a refrigerated area.

2.1.2: Cellulose Nanofiber Synthesis

Cellulose nanofibers were synthesized according to Saito et al. (29). The cellulose was first TEMPO-oxidized. 1 g of bleached kraft pulp was added to a beaker with 100 mL of water, 0.016 g of TEMPO, and 0.1 g of NaBr. 2.1 mL of 1.8 M NaClO was then added to the suspension and the pH was kept at 10. The suspension was thoroughly mixed for 1 hour and then washed with water to produce TEMPO-oxidized cellulose.

100 mL of 1% $NaClO_2$ was then added to the TEMPO-oxidized cellulose at a pH of 4.8 for 24 hours and washed with water. The suspension was diluted with water and mechanically pulverized using a microfluidizer. The suspension was centrifuged to remove large fibers and the supernatant was kept as the cellulose nanofiber dispersion.

2.1.3: Gelatin Synthesis

Gelatin powder was added to a beaker with water to make a 10 mg/mL solution. The solution was covered, heated to 45 C, and stirred until all the powder was dissolved. The beaker

was then allowed to cool to room temperature before using. The gelatin solution was made fresh and was not stored.

2.2: Aerogel Fabrication

An OT-2 pipetting robot (Opentrons, USA) was used for automatic pipetting of aerogel materials into various recipes. A benchtop vortexer was used for mixing samples. Silicone molds were purchased from Amazon. Glutaraldehyde was purchased from Sigma Aldrich.

2.2.1: OT-2

MXene, gelatin, and cellulose nanofiber suspensions were prepared as 1 wt% suspension in 50 mL conical tubes and placed in the OT-2 material slot. Empty 15 mL tubes were labeled and placed in the provided tube racks in the sample slots in the instrument. Recipes were prepared according to the machine learning model suggestions and the recipes for each batch were input into the OT-2 software.

2.2.2: Aerogel Preparation and Freeze-drying

Once the OT-2 was finished adding the required amounts of MXene, gelatin, and cellulose nanofibers to the 15 mL conical tubes, the tubes were capped and removed from the instrument. Glutaraldehyde was then added to sample tubes per each recipe's requirements and the tubes were vortexed at 3000 rpm for 3 minutes. Sample suspensions were transferred into 0.6"x0.6"x0.4" molds, generally samples were split into three mold wells, and refrigerated overnight. Samples in molds were flash frozen in liquid nitrogen then placed in a benchtop freeze-dryer (Labconco, USA) for 4-5 days until all the ice was removed from the samples. Once the aerogels were completely dry, they were removed from the molds and stored for characterization and testing.

Aerogel recipes for further testing were prepared as before but with manual pipetting of each recipe component instead of using the OT-2. For further joule heating tests, sample molds were the same as before. For thermal conductivity testing, sample molds were larger 2”x2”x1” and 4”x4”x4” silicone molds, where the overall sample volume increased but the sample composition and concentration stayed the same.

2.2.3: Measuring Aerogel Size and Height

The aerogel surface area was measured using imageJ and the height was measured prior to compression testing using the Instron tensile tester.

2.3: Resistance Measurement

After compression testing, the resistance of each aerogel sample recipe was measured by fabricating electrodes onto glass slides and mounting aerogel samples to those devices. Devices were made from glass slides, VHB tape, copper tape, and silver conductive paint, as shown in Figure 5.

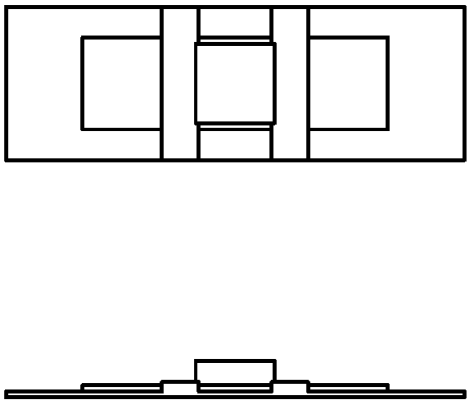

Figure 5: Diagram of the resistance measurement device.

2.3.1: Fabricating Device for Resistance Measurement

Each aerogel recipe sample was mounted to its own individual device. was created by mounting a short strip of VHB tape to the center of a glass slide. Electrodes were then pasted on top by using strips of copper tape, placing them perpendicular to the long side of the glass slide, and keeping the distance between the electrodes fixed at 1.2 cm.

2.3.2: Measuring Resistance and Determination of Appropriate Aerogel Recipes

Resistance was measured by connecting a Fluke Multimeter to the electrodes of the aerogel. Resistance was measured three times to ensure good contact between the alligator clips of the Multimeter and the electrodes on the sample device.

2.4: Compression and Sensitivity Measurements

The pressure an aerogel recipe experiences at 30% compression (strain) was measured using an Instron. Samples were compressed at a rate of 0.02 mm/s until the aerogel height was compressed by 30% of the starting height. Samples were then decompressed back to the starting height at a rate of 0.02 mm/s. This cycle was repeated 5 times in total and the stress and strain values were recorded. Maximum pressure values at each cycle were extracted from the data for further analysis.

To measure the sensitivity of an aerogel to a force or pressure applied to it, the aerogel was mounted to a device, similar to that for measuring resistance. Electrodes from the device were connected to a MeterOhm Autolab electrochemical workstation, and a constant voltage of 0.01 V was applied to the sample. Pressure was applied to the sample, similar to when measuring E_{30} values, where samples were compressed at a rate of 0.02 mm/s.

The current over time was plotted against the sample pressure and sensitivity in terms of current and resistance was calculated as follows:

$$S_I = \frac{\frac{R_0 - R}{R_0}}{P - P_0} = \frac{\frac{I - I_0}{I_0}}{P - P_0}$$

where, R_0 is the sample's initial resistance, R is the measured resistance, P is the applied pressure, P_0 is the initial pressure (in this case 0), I is the measured current, and I_0 is the initial current.

2.5: Joule Heating and Temperature Measurement

2.5.1: Connecting Thermocouple to Aerogel Device

The tip of a type K thermocouple was placed approximately 1 mm into the side of the aerogel sample above the electrode connection. The wire of the thermocouple was mounted to the resistance device to prevent the thermocouple tip from becoming dislodged from contacting the aerogel sample. Silver conductive paint was placed where the thermocouple tip meets the surface of the aerogel to provide good contact between the aerogel and the thermocouple for accurate temperature measurement. The silver paint was dried overnight before temperature tests were conducted.

2.5.2: Voltage vs. Temperature of Aerogel Measurement

The aerogel device was connected to the MeterOhm Autolab and the thermocouple was connected to a temperature data logger. Voltages between 0 and 5 V were applied to the aerogel sample for 5 minutes and then removed for 5 minutes to allow the sample to return to room temperature. Sample temperature was recorded for the sample heat-up and cool-down cycle.

Sample temperature during heating was also measured using a thermal IR camera to confirm that the thermocouple was making good contact with the sample.

2.5.3: Cyclic Heating with and without Compression

The aerogel device was then placed onto the Instron sample platform and different sample compression strains were applied, starting from 0% to 20% strain. At each compression, the device was connected to the Autolab and voltage was applied for 100 seconds and removed for 100 seconds. This cycle was repeated 100 times to test aerogel heating stability over time, and temperature was measured and recorded over the entire 100 cycles.

2.6: Thermal Conductivity Testing

Sample thermal conductivity was measured using a Thermtest Instruments HFM-25. A NIST calibration sample and data sheet was provided by Thermtest. The HFM-25 has a minimum testing sample size of 50 x 50 x 2 mm and a maximum testing sample thickness of 25 mm.

2.6.1: HFM-25 Instrument Calibration

Prior to testing any aerogel samples, the HFM-25 was calibrated using the provided NIST 1450E sample. The NIST 1450E sample thickness was determined by measuring each side three times using a caliper and taking the average of all the values. The sample clamping area was cleared of all debris, the sample was inserted into the HFM-25, and the 1 kg weight was placed on top of the upper plate. The sample material name was entered into the software, which auto populated the calibration test, and the sample thickness was entered into the software.

When all the parameters were input into the software, the calibration was started. Two temperature deltas were measured: 17.5 to 32 C and 15.0 to 35.0 C. Both temperature deltas had

a mean of 25.0 C. The measured thermal conductivity of the standard was compared with the reported thermal conductivity specified on the data sheet to confirm that it is within 0.33% of the reported value.

2.6.1: Sample Thermal Conductivity Testing

Once the instrument is calibrated, it is ready to be tested. 2”x2”x0.8” samples were placed in between the plates with spacers the height of the sample placed at the edges of the two plates to prevent the sample from collapsing completely during testing. The 1 kg weight was then placed on top of the instrument plates. The thermal conductivity at room temperature was measured with temperature deltas of 17.5 °C and 32 °C at each plate.

3: Machine Learning for Recipe Determination

Due to the large amounts of data that can be collected and that already is available, scientists are interested in quicker ways to predict or screen new materials for applications of interest. To use this technology for recipe prediction for conductive aerogels, a machine learning model was trained on the measured aerogel resistance data similar to the process used by Yang et. al. (30). In brief, a boundary for the model was set by categorizing the resistance data into electrically conductive and not conductive samples, and then a support vector machine classifier was trained via active learning cycles.

3.1: The Need for Machine Learning in Aerogel Recipe Design

Aerogels comprising of MXene, gelatin, and cellulose nanofibers need to successfully form aerogels from a solution of solids in water in order to be usable for applications, such as wearable heaters. In the process of fabricating aerogels for personal thermal management, four degrees of freedom (DOF) were explored: composition of MXene, cellulose nanofibers, and gelatin which provided for two DOF, mass loading provided one DOF, and the presence or absence of a cross linker was the fourth DOF. As there are many changing variables, the design space of feasible and infeasible aerogels needs to be explored and characterized. Once the space of feasible aerogel recipes is defined, the machine learning prediction model can be trained to suggest recipes that can form successful aerogels with desired properties.

3.2: Boundary Definition using a Support Vector-Machine Classifier

3.2.1: What is a Support Vector Machine?

It is necessary for the machine learning model to recommend recipes that can form structurally intact aerogels that can then be used in further rounds of active learning. A support

vector machine (SVM) assigns labels to objects to learn and classify materials into a set amount of groups or labels. An SVM is a computer algorithm used to categorize or label data by learning from training or example data (31). It uses supervised learning to build a data classifier model through defining a hyperplane, which separates the data into groups with the widest boundary between data groupings.

3.2.2: Grading Aerogels

As the design space of the materials of interest is large, the boundary of what recipes will produce successful and failing aerogels needs to be defined. The SVM was trained to recognize different aerogel formation cases which are sorted into feasible and infeasible cases. Aerogels that could be removed from the molds and formed solid monolithic structures were classified as an "A" grade aerogel. Aerogels where the structure is mostly continuous but contains cracks and fragments were classified as "B" grade. When the aerogel has some structural continuity but is mostly flakes or crumbles, it is classified as "C" grade. Aerogels with no structure and are all flakes are classified as "D" grade. Out of these classifications, recipes that produce "A" and "B" grade aerogels are considered feasible, and recipes that produce "C" and "D" grade aerogels are infeasible. Recipes that cannot successfully form aerogels are not able to be used for successive testing and characterization.

3.2.3: The Need for a SVM

By training an SVM, the model can define the boundary between feasible and infeasible recipes, and only suggest recipes in the feasible region. This screens out recipes that not only have a low probability of not forming monolithic structures, but allows for recipes to be suggested that will be robust enough for applications. It is possible to use a design of experiments style matrix to fabricate aerogels with systematic compositions of materials, grade

each aerogel, and then use the aerogels that fall in the feasible region as the design space. However, that design space classifier would contain recipes that fall on the border of feasible and infeasible, leading to the possibility of the model suggesting a recipe that does not form a continuous aerogel and would thus be not usable for applications. If the border of feasible and infeasible recipes had a stricter cut-off to guarantee recipes that are able to form complete aerogels with no cracks or crumbling, the model may overlook recipes that are right at the border of feasible and infeasible and would exclude potential recipes.

A support vector machine divides data into groups, where the separation between groups is as large as possible. In general, the SVM creates a hyperplane or set of hyperplanes in the space where all the data points lie to classify new data points. In a two-dimensional dataset, this divider would be a line that curves between the two groups, and in a higher-dimensional (n-dimensional) dataset, the divider would be a plane or hyperplane with n-1 dimensions. Aside from classification, a SVM can also use the hyperplane for regression and determining outliers in a dataset.

3.2.4: Training an SVM Classifier Model

A SVM was trained based on the feasible or infeasible recipes to make sure the model knows to recommend recipes that have a high chance of forming aerogels that will not crumble. The SVM is then created by selecting a kernel function to maximize the separation between data groups as opposed to using dot products to fit the hyperplane. Common kernels are homogeneous and inhomogeneous polynomials, Gaussian radial basis functions, and sigmoid functions. For the model used here a radial basis function was used to process the non-linear data. Then the SVM model was trained using recipes and feasibility grades so it can "learn" what recipes to suggest. Finally, the SVM is optimized to adjust the classification.

Kernel machines are used for pattern analysis and are useful for operating in higher dimensional spaces by computing the inner products between the images of the data pairs in the space. The radial basis function can be used as the kernel function in the SVM as it uses the distance between the input values and a fixed value, generally a kernel at the center or origin. The radial basis function is a widely used kernel as it is similar to the Gaussian distribution and can calculate how similar two points are. It aims to minimize the value of the kernel by determining an appropriate weight for the function.

After the kernel function is selected, the data points are entered to train the machine, and the function is further optimized. Matthew's correlation coefficient is used to optimize the classifier model as it is a statistical tool that can use a generated random guess to evaluate if the prediction model is better or worse than a random guess. Matthew's correlation coefficient (MCC) is defined as the following:

$$MCC = \frac{TP \times TN - FP \times FN}{\sqrt{(TP + FP)(TP + FN)(TN + FP)(TN + FN)}}$$

where, TP is true positive, TN is true negative, FP is false positive, and FN is false negative.

3.3: Active Learning and Data Augmentation

The second step in training the machine learning prediction model was to use active learning in combination with data augmentation using the resistance data collected. The model was based on an artificial neural network (ANN), which mimics the way humans think and learn. The ANN has a set of nodes that are similar to the neurons in a brain in that they are connected to other nodes similar to synapses. A node will have an input or multiple inputs, will then process that signal, and will send a signal to the surrounding nodes, which will do the same until the signal reaches the output node or nodes. The nodes are organized into many interconnected

layers and information or signals travel one way through this network. As the signals travel through the network the weights and thresholds at each node are changed to optimize the prediction model's accuracy. This is through maximizing or minimizing a mathematical function, such as minimizing the mean relative error or mean absolute error between the machine learning model's predicted values and experimental values.

As the range of resistance values is very large, spanning many orders of magnitude, and we are only interested in recipes producing low resistances values under 200 Ohms, the prediction model was trained on the logarithm of resistance (32). 131 aerogel samples were fabricated with the assistance of the OT-2 robot to increase production efficiency, and their electrical properties were measured. The resistance data collected ranged from 0 to 99,999,999 Ohms and also included "overload" results, where the resistance value of the recipe was too large to be measured by the Fluke Multimeter. These 131 recipes were divided into two categories: measurable and immeasurable recipes for applications requiring highly conductive aerogels. Measurable, or feasible, recipes are those with resistance values equal to or below 200 Ohms, and immeasurable recipes are those with resistances greater than 200 Ohms. Of the recipes tested, 36 recipes yielded feasible resistance values and 95 recipes yielded infeasible resistances for electrically conductive aerogels. "Overload" resistance values were input into the model as very high resistances of 100,000,000 Ohms to include a quantifiable resistance value for these non-conductive recipes. The data, which includes the specific composition of recipes and their corresponding resistances, was input into the model to train it on what recipes have resistances under 200 Ohms.

3.3.1: Data Augmentation

To further increase the prediction model's accuracy, the experimental data points were augmented to generate virtual data points that the model could be further trained on. The virtual data points are made from minor changes to the existing data and it reduces the chances of the model overfitting to the existing dataset. Similar to Yang et al., virtual data points can be generated via the Synthetic Minority Oversampling Technique for REGression (SMOTE-REG) and via the User Input Principle (UIP). This adds more data for the model to be trained on without the need to generate more experimental data.

3.3.2: Evaluating the Model's Accuracy

The third step is to test the prediction model's accuracy. The model was evaluated using a separate set of testing data that was not input into the artificial neural network for the model. A total of 11 compositions and measured resistances were input into the model and the model predicted the resistance values for these compositions. The mean relative error was used to describe the model's accuracy during active learning cycles; the active learning process ends when the mean relative error (MRE) stabilizes, defined in the equation below.

$$MRE = \frac{1}{N}\sum_{i=1}^{N}\left|\frac{output^i - \log E^i}{\log E^i}\right|$$

N is the total number of testing data, $output^i$ is the predicted output value from the model, logarithm of resistance in this case, and $\log(E^i)$ is the measured experimental output, which is the logarithm of the measured resistance. A high prediction accuracy of the SVM using log R was achieved as the amount of data input into the model increased (Figure 6).

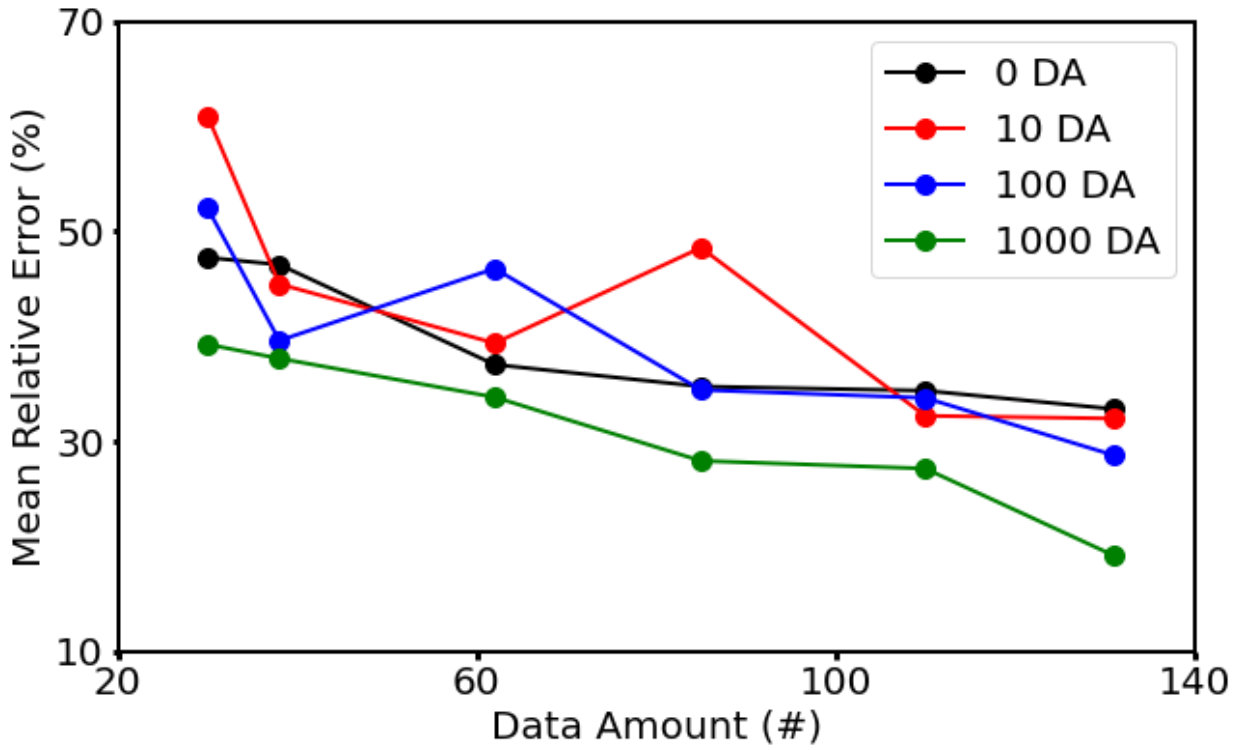

Figure 6: The Mean Relative Error (MRE) of different prediction models based on the data augmentation ratio (number of virtual-to-real data points).

As the number of data input into the model increases, the mean relative error of the prediction model decreases, which indicates that the accuracy of the model increases. Increasing the data augmentation value also increases the model prediction accuracy. The most accurate model trained includes the full 131 measured data points and a virtual-to-real data ratio of 1000, and this gave a low MRE of 19%. As the data augmentation number increases, the time to train the model increases.

3.4: Comparing the Artificial Neural Network Model with Common Machine Learning and Statistics Models

Linear regression is commonly used in statistics to predict values based on fitting a linear model to the data set. Decision trees, random forests, gradient-boosted decision trees, and artificial neural networks are machine learning tools also used by fitting the experimental or

observed data to a model, but this is not necessarily a linear fit. Decision trees are models based off a set of rules, but they suffer from over or under-fitting data. This can be solved by random forest models where the number of decision trees are reduced, but the diversity of trees is increased, so the sum of rules can be incorporated into the model (33). A gradient-boosted decision trees model is similar to random forest but builds the group of decision trees one tree at a time and combines results as the process happens (33). The prediction model from the artificial neural network was compared with other prediction models based on linear regression, decision tree, gradient-boosted decision tree, and random forest (Figure 7).

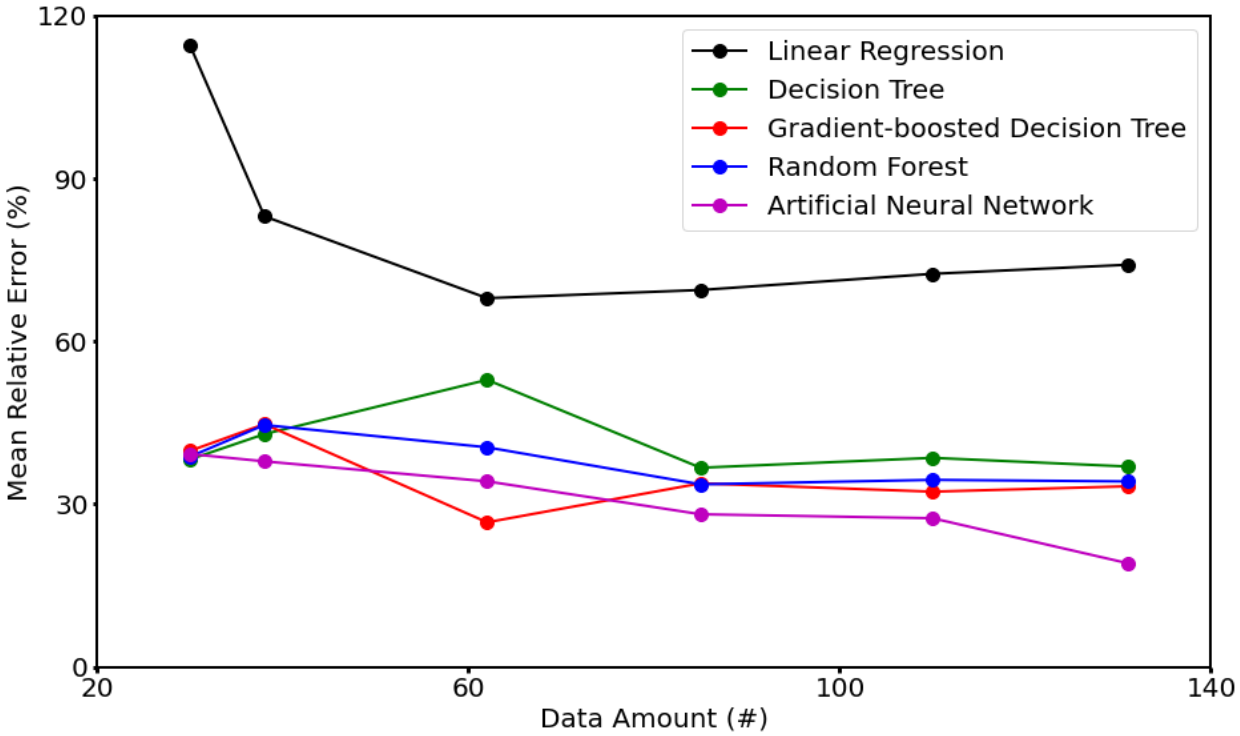

Figure 7: Comparing the predictive power of the artificial neural network to linear regression and other machine learning models.

The machine learning models have a higher predictive power compared to statistical analysis models using linear regression. Among the algorithms using decision tree, gradient-boosting decision tree, random forest, and artificial neural network (ANN), they all are more

accurate models compared to the linear regression model, but the ANN model has the lowest MRE and thus the highest accuracy.

3.5: Interpreting Machine Learning Model Results

There are many features or parameters that are varied in the aerogel recipes: the percent of MXene, cellulose nanofibers, and gelatin, the presence or absence of glutaraldehyde, and the weight percent of the aerogel. Due to the high DOF of the system, typical data analysis methods may be difficult to determine underlying trends of the parameters effect on the recipe's resistance.

3.5.1: Initial Data Analysis

To gauge initial trends, the data can be split into groups with and without cross linker at each concentration and the effects of two of the three components MXene, cellulose nanofibers, and/or gelatin can be graphed against the conductance, which is the inverse of the resistance. Figure 8 shows the correlation of resistance vs CNF and MXene amount for recipes not including the crosslinker and separated by mass loading. Due to the high DOF, it is difficult to also plot all three components MXene, cellulose nanofibers, and gelatin and also see their effects on the overall resistance.

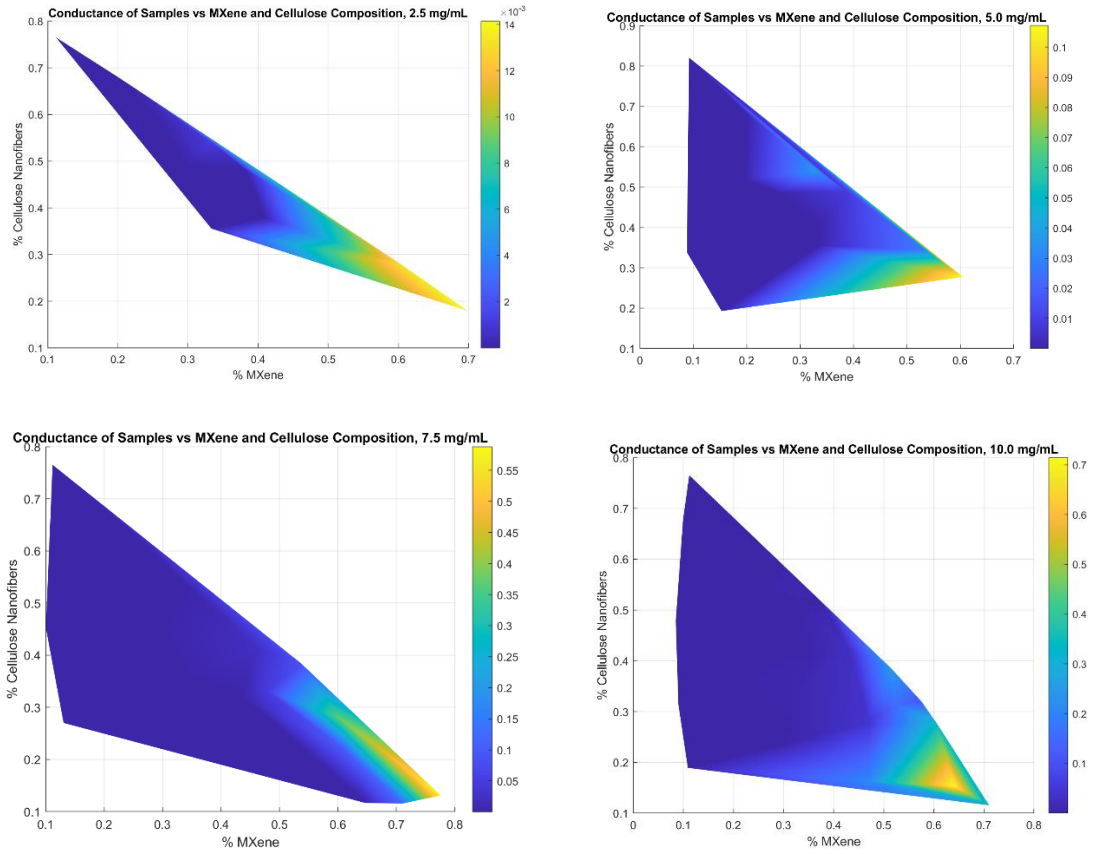

Figure 8: The correlation of percentage of MXene and cellulose nanofibers son the conductance for uncrosslinked recipes.

Delaunay triangulation was used to generate the space between each data point to assist in visualization of the conductance data between each data point. It is clear to see that more MXene and less cellulose nanofibers leads to lower resistances and higher conductance values for the uncrosslinked recipes. It is then necessary to see if adding glutaraldehyde has an effect on the conductance, so the correlation of MXene and cellulose nanofibers on the conductance with crosslinker added was explored (Figure 9).

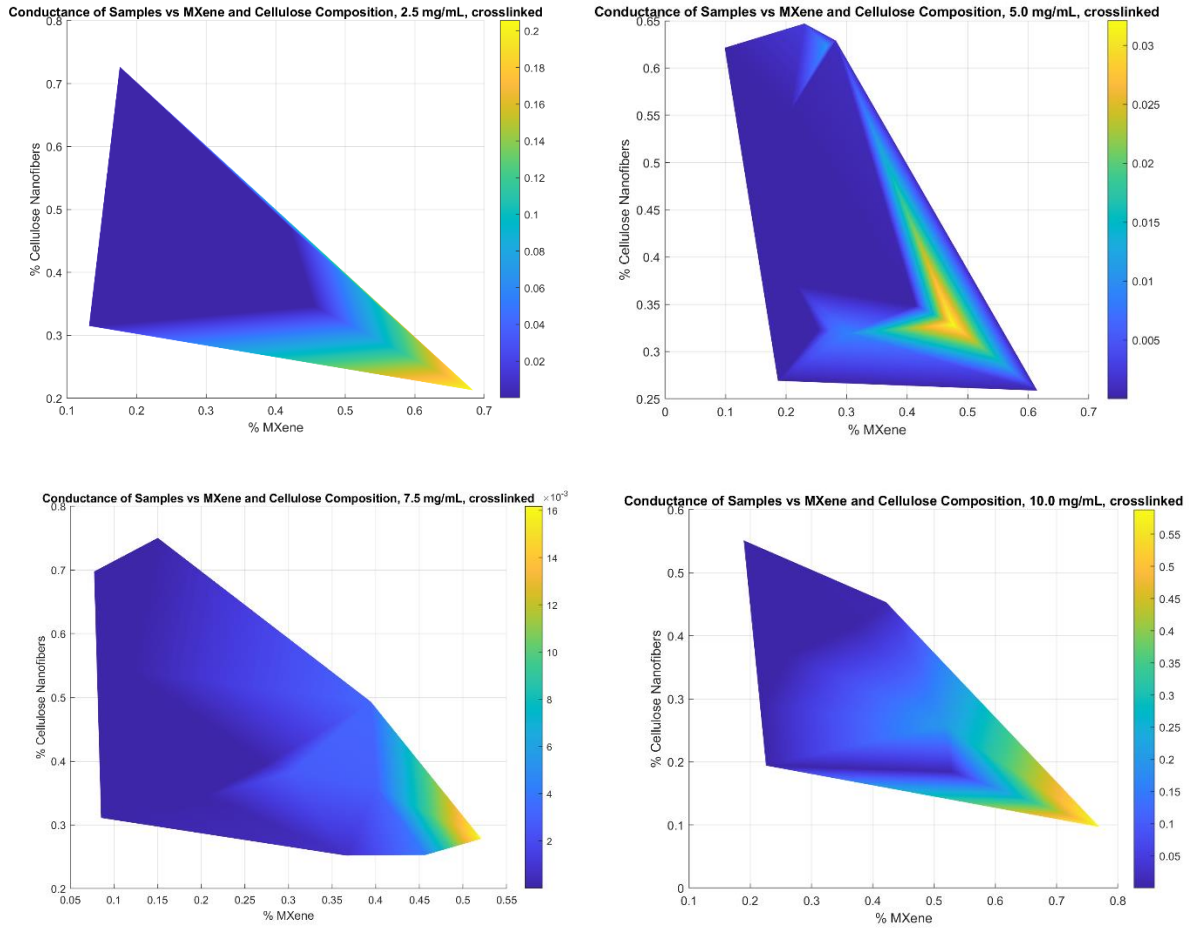

Figure 9: The correlation of percentage of MXene and cellulose nanofibers son the conductance for crosslinked recipes.

It is also apparent that more MXene compared to cellulose in the crosslinked samples leads to better conductance. However, it appears that including the crosslinker has little to no effect on the conductance.

3.5.2: SHAP

By using Shapley Additive Explanations (SHAP), is possible to determine how much each feature of the recipe contributes to the overall resistance (or conductivity) of each aerogel sample (30). The Shapley values estimate how important a feature contributes to the output property through the magnitude of the value and whether or not the feature positively or negatively contributes to the output, a positive or negative sign respectively (34). Thus, a

narrower range of SHAP values correlates to a feature that is less important to the output and a wider range correlates to a feature that is more important. The SHAP data was determined for the conductive aerogels, where the features were separated into percent of cellulose nanofibers, percent of MXene, percent of gelatin, mass loading, and absence or presence of glutaraldehyde (Figure 10).

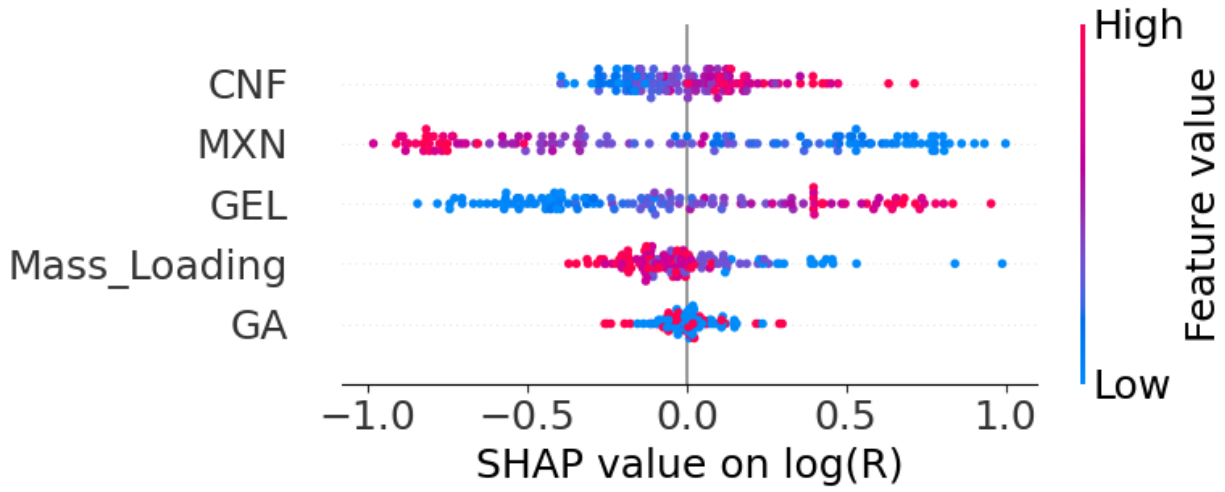

Figure 10: Overall SHAP data correlating features on their impact on the output, which is the log(R).

A high log(R) value indicates a low resistance, which is desirable for wearable heaters. From the SHAP data, it is observed that a high amount of MXene has a negative correlation on log(R), which indicates that more MXene leads to more desired resistance values. The SHAP values of MXene and gelatin span from -1.0 to +1.0 and -0.9 to +1.0 respectively, showing that these components are influential on the output of log(R). The SHAP values of cellulose nanofibers and the mass loading span from -0.5 to +0.8 and from -0.4 to +1.0 respectively, which indicates that these components were less influential and also had opposite effects on the log(R) output. The SHAP values showed no correlation between the presence or absence of glutaraldehyde on log(R).

Further dividing the overall SHAP data by concentration, similar trends can be observed in Figure 11.

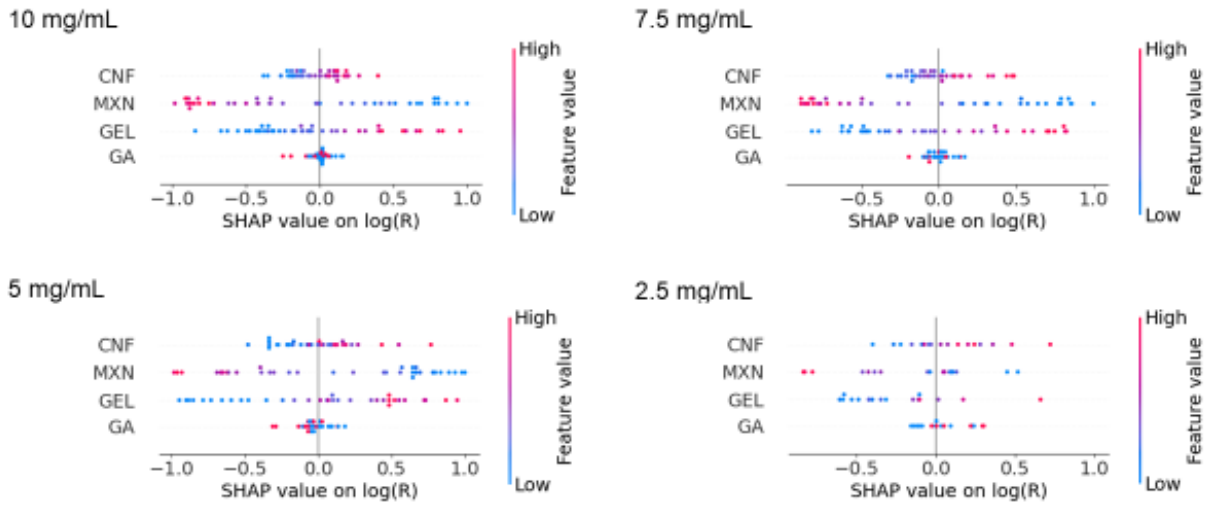

Figure 11: SHAP data separated out by mass loading.

Regardless of concentration, the amount of MXene and gelatin continues to have a strong impact on the resistance of the material, the amount of cellulose has a moderate effect on the resistance, and glutaraldehyde has no effect on the resistance.

4: Data Analysis

4.1: Summary of Resistance Data

The resistance data for all samples tested are graphed as a measure of their conductivity as a function of composition. Sample resistances ranged from 1 to 50,000,000 Ohms and included samples where the resistance was too high to be measured using the Multimeter. To more easily separate recipes with lower resistances, the sample's conductance, its inverse resistance, was graphed. Data was separated based on sample concentration and presence or absence of the crosslinking agent glutaraldehyde. A clear trend was observed for the composition of MXene in the sample, as seen in Figure 12.

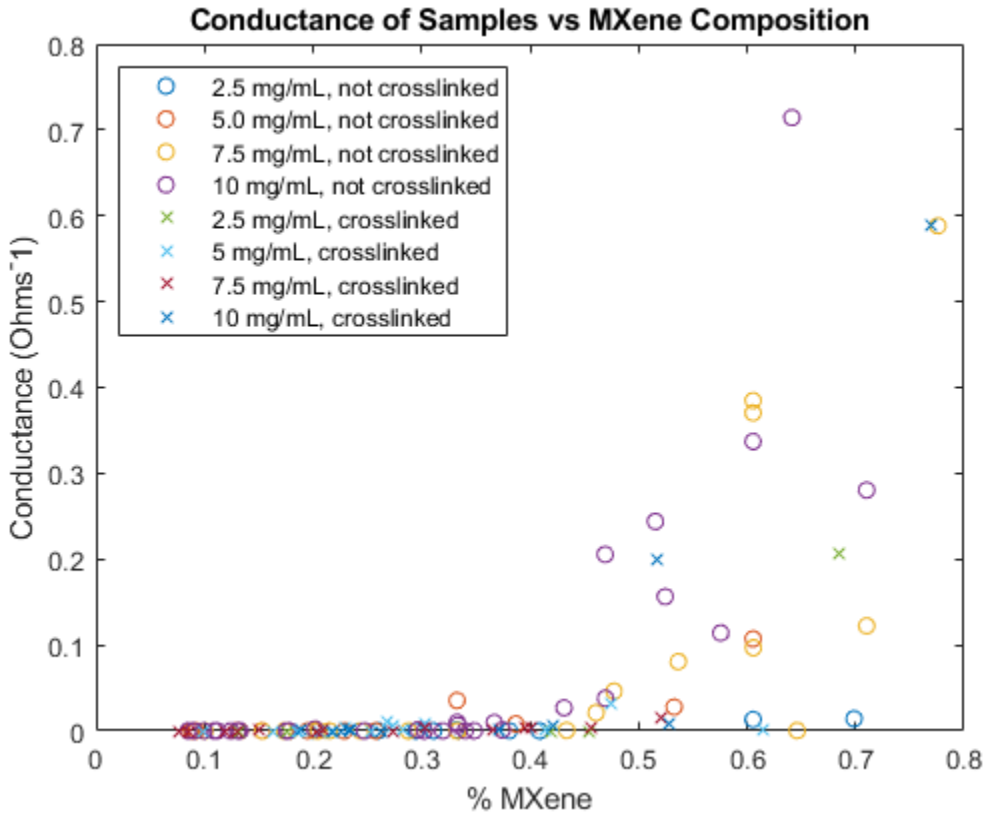

Figure 12: The correlation of percent MXene in each sample on that sample's conductance.

It can be seen that as the percent of MXene increases, the conductance also increases. Sample recipes with conductance greater than 0.01 $Ohms^{-1}$, corresponding to resistances less than 100 Ohms, were further tested to determine their suitability for personal thermal management applications.

4.2: Summary of Sensitivity Data

The samples with resistances less than 100 Ohms were then further tested to determine promising samples that are strain insensitive but are still electrically conductive.

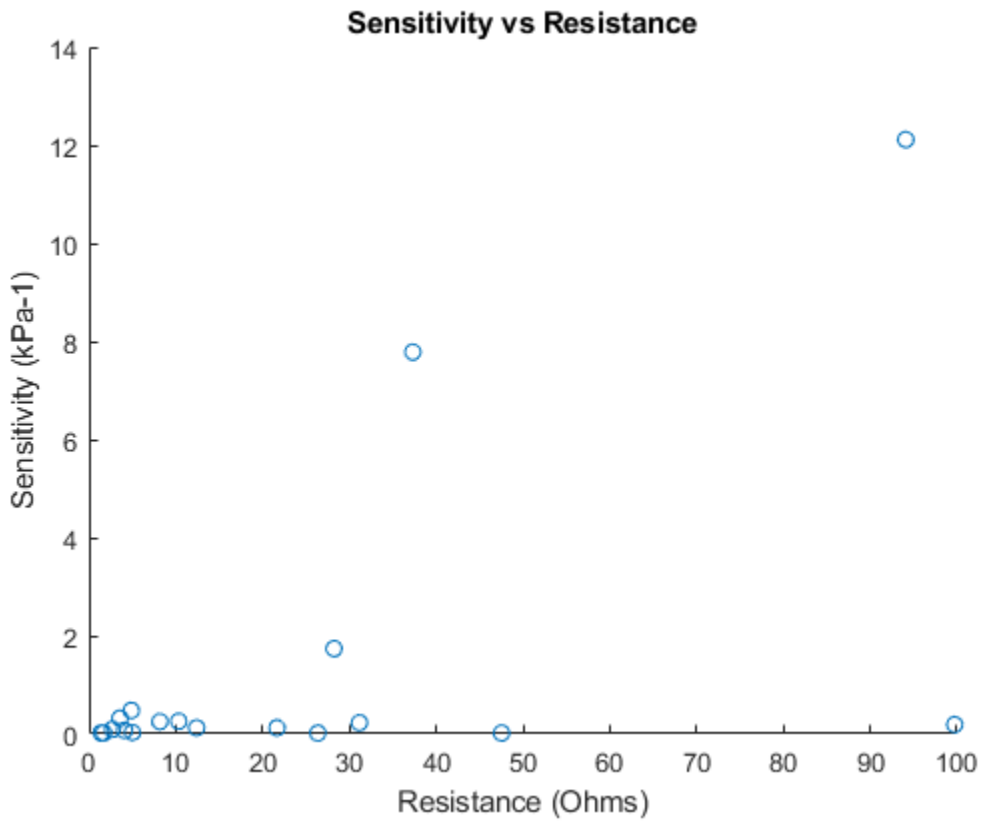

Figure 13: Sensitivity versus recipe resistance for the conductive aerogel recipes.

From Figure 13, it was found that most of the samples with low resistances under 20 Ohms also have sensitivities below 1 kPa^{-1}. The recipe from sample C30B with 13% cellulose nanofibers, 78% MXene, 9% gelatin, a concentration of 7.5 mg/mL, and no crosslinker had a

resistance of 1.7 Ohms and a sensitivity of 0.02 kPa^{-1}. This recipe was chosen as a promising recipe for a strain insensitive material. For comparison, a low resistance but more strain sensitive recipe was selected. The recipe from sample C105 with 12% cellulose nanofibers, 71% MXene, 17% gelatin, a concentration of 10 mg/mL, and no crosslinker had a resistance of 3.56 Ohms and a sensitivity of 0.32 kPa^{-1}. For use in wearable heaters, it is important to have strain insensitive materials to prevent large increases in resistance when compression is applied, which would lead to higher than expected temperatures.

4.3: Strain Insensitive Sample for Wearable Heaters

4.3.1: Cyclic Compression Stability Testing

The resistance of the aerogel sample was monitored over time for 100 compression cycles at a strain rate of 20% of the sample height. A good sample for joule heating applications for personal thermal management will have minimal change in resistance under compression and repeated cycles of loading and unloading the force should not change the minimum and maximum resistances of the sample by a significant amount. The relative resistance indicates how the resistance changes with respect to the starting sample resistance.

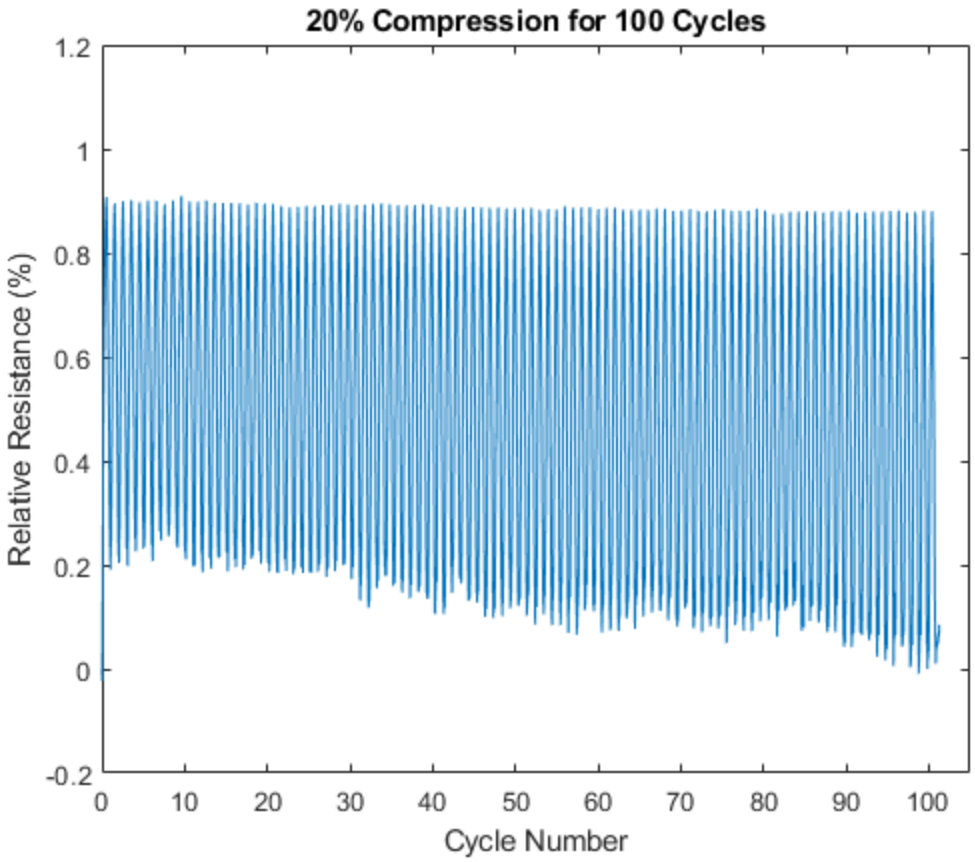

Figure 14: Relative resistance as a function of compression cycle number for 100 cycles at 20% compressive strain.

The relative resistance starts out at 0, meaning that the deviation from the starting resistance is 0, and as compression is applied to the sample, the relative resistance increases by 0.9% of the starting resistance. Since the resistance of this sample is already very low, the 0.9% increase in relative resistance is not large enough to negatively affect the sample for joule heating applications. Over the 100 cycles, the maximum change in relative resistance is consistent at 0.9% and the minimum resistance stays within 0 to 0.3%.

4.3.2: Joule Heating Temperature Range for the Strain Insensitive Sample

A range of low voltages, under 5 V, were applied to the aerogel sample to determine an appropriate voltage for thermal management for human centered applications. The temperature

of the aerogel sample was recorded to observe the heating profile of the material over 300 seconds of applying the voltage, and the return to room temperature was observed for 300 seconds following removal of the voltage (Figure 15).

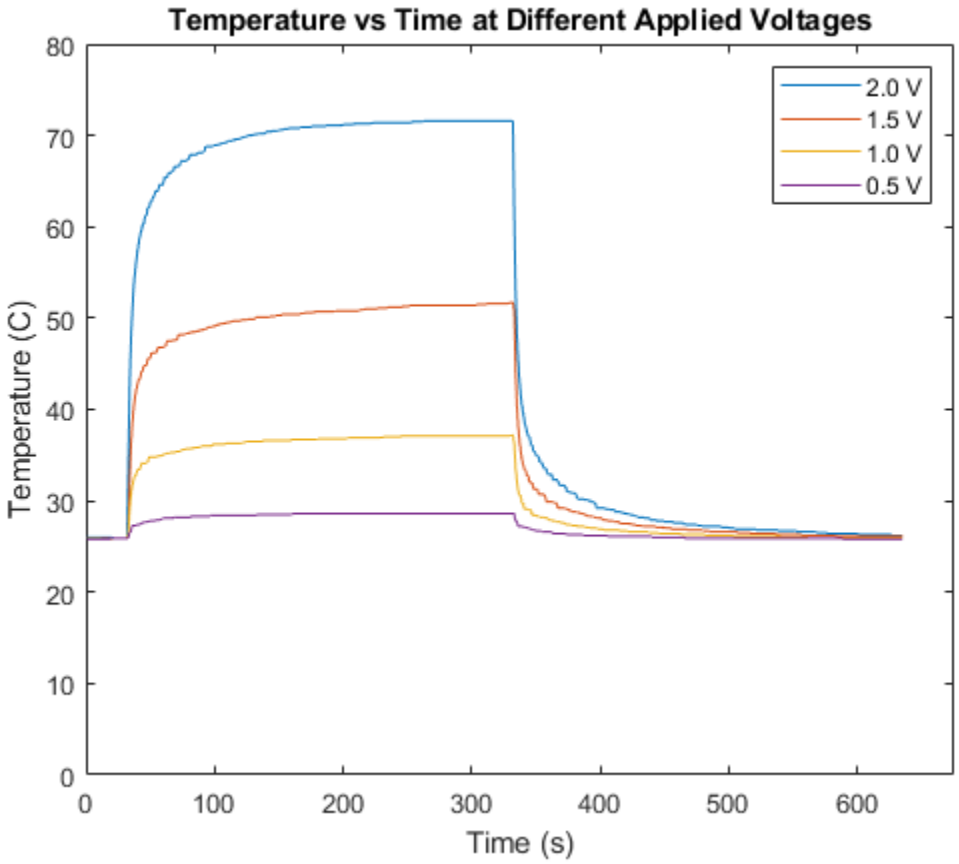

Figure 15: Temperature versus time for recipe C30B when applying voltages of 0.5, 1, 1.5, and 2 V.

When voltage is first applied, the aerogel responds quickly and has a sharp increase in temperature within a few seconds. After approximately 100 seconds, the temperature starts to plateau and the temperature increase after an additional 200 seconds is less than 5%. At 0.5, 1, 1.5, and 2 V the maximum temperature reached is 28.6, 37.2, 51.7, and 71.6 C respectively.

To determine if the material follows Joule's law, the maximum temperature was plot against the squared voltage (Figure 16).

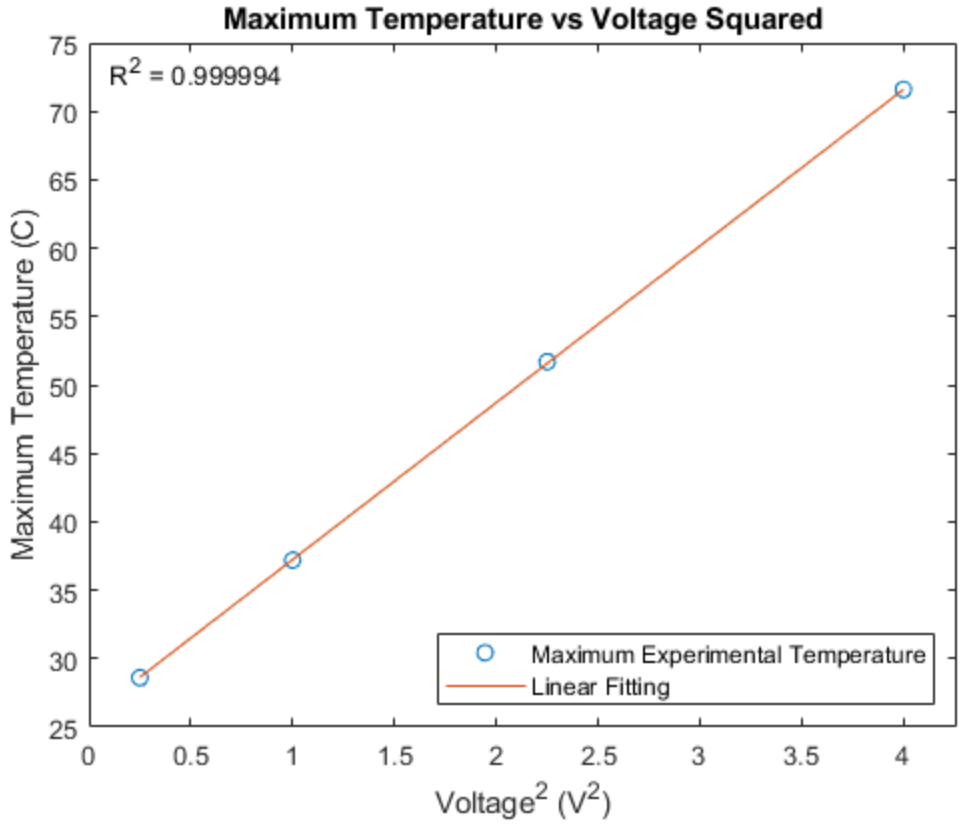

Figure 16: Linear fitting of the squared voltage versus the maximum temperature of the material at that voltage.

According to Joule's law, the power output, in this case the maximum temperature, is proportional to the square of the energy input, which is the applied voltage. The data follows a linear trend with an R^2 of 0.999994.

4.4: Cyclic Joule Heating Stability on Strain Sensitive and Insensitive Samples

4.4.1: 1 Volts Applied to the Strain Insensitive Sample

The temperature stability of the samples over multiple cycles of heating and cooling was tested with and without 20% compression. Each cycle consists of 100 seconds of heating and 100 seconds of cooling. 1 V was applied to and removed from the strain insensitive sample for 100 cycles and the temperature response was monitored (Figure 17).

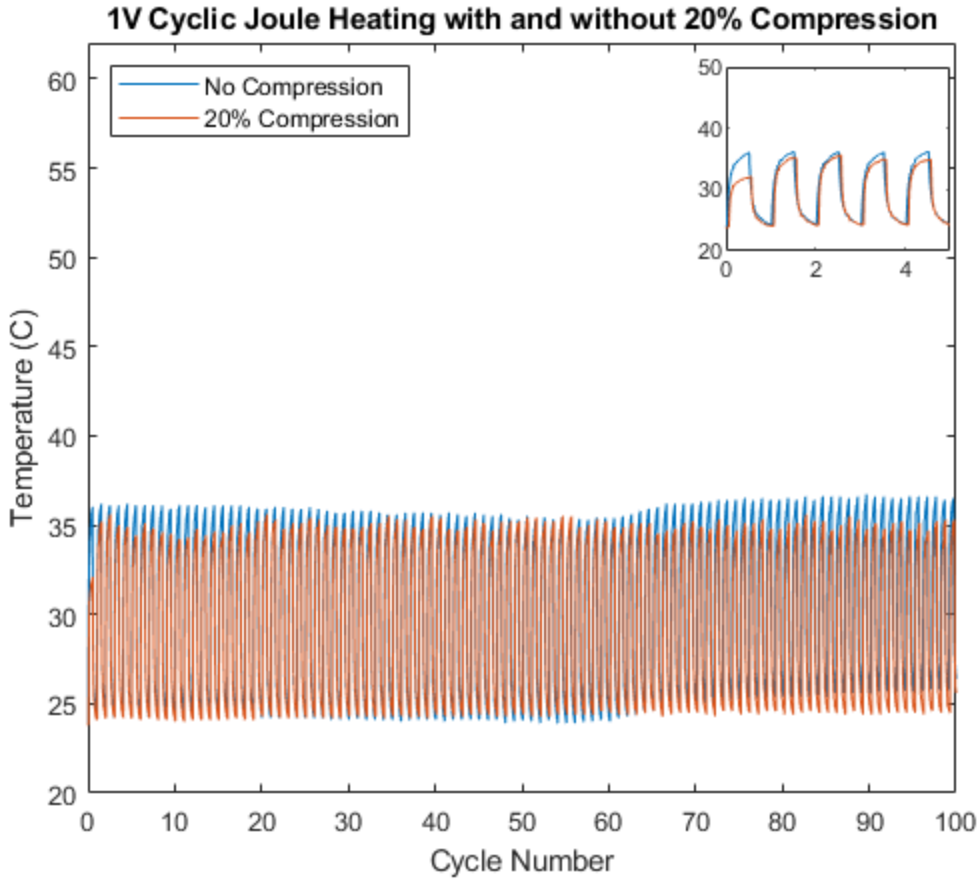

Figure 17: Cyclic joule heating of the strain insensitive sample, C30B, at 1 V with and without 20% compression.

The maximum temperature of the sample after 100 seconds at 1 V without compression is 36 C and the maximum temperature when the sample is under compression is 35 C. The sample is able to return to room temperature in each cycle with minimal drift in temperature under both compression and no compression cases.

4.4.2: 1.5 Volts Applied to the Strain Insensitive Sample

The temperature stability was also tested at higher voltages to see if there is temperature drift or if the temperature greatly changes under compression (Figure 18).

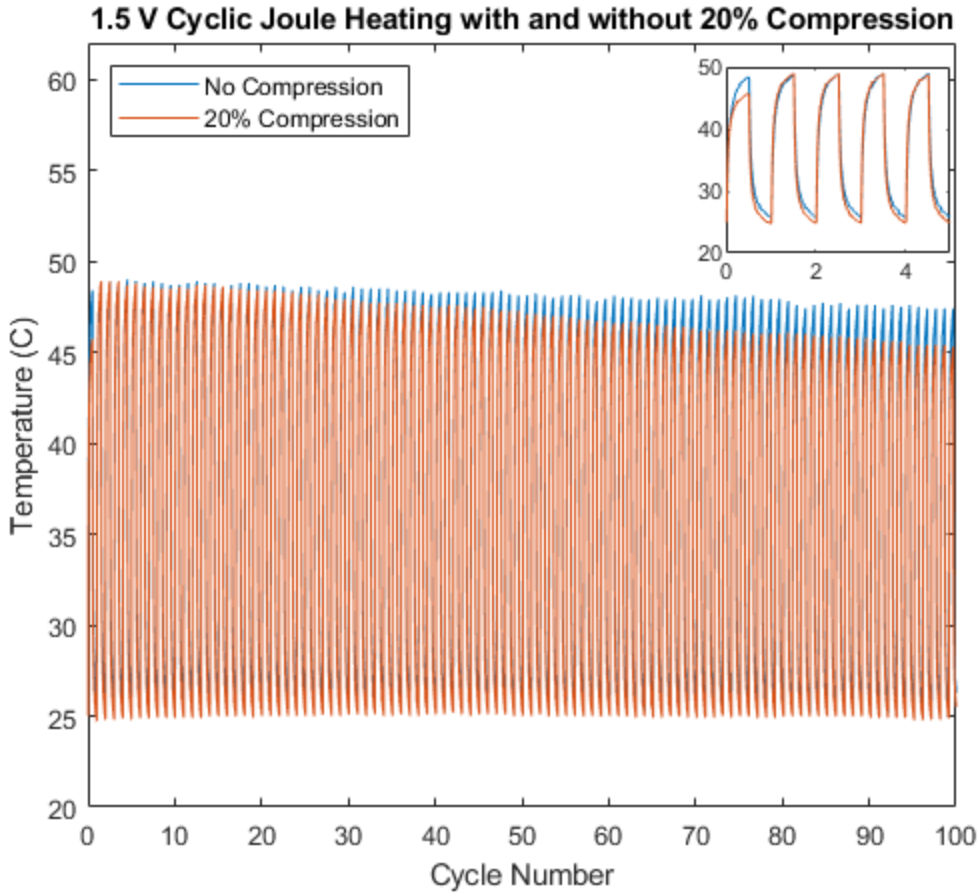

Figure 18: Cyclic joule heating of the strain insensitive sample, C30B, at 1.5 V with and without 20% compression.

The maximum temperature reached in the first few cycles of the sample both with and without compression is 48 C. Since the recipe is strain insensitive, the resistance does not change much with compression. According to Joule's law, the temperature is inversely proportional to the resistance. As the resistance of the sample did not change with compression, the temperatures in the first few cycles of heating and cooling matched. However, after 20 to 30 cycles, the maximum temperature of the sample under compression starts to decrease and is 45 C in the final cycle compared to 47 C for the sample not under compression.

4.4.3: 1 Volt Applied to the Strain Sensitive Sample

The temperature stability over 100 cycles was tested for a more strain sensitive sample than that of C30B. Recipe C105 is composed of 12% cellulose nanofibers, 71% MXene, and 17% gelatin, does not contain glutaraldehyde as a crosslinker, and has a concentration of 10 mg/mL. This recipe has a low resistance of 3.57 Ohms but has a higher sensitivity of 0.32 kPa^{-1} compared to 0.02 kPa^{-1} for the strain insensitive recipe. 1 V was applied to this strain sensitive sample for 100 cycles of heating and cooling for no compression and 20% compression (Figure 19).

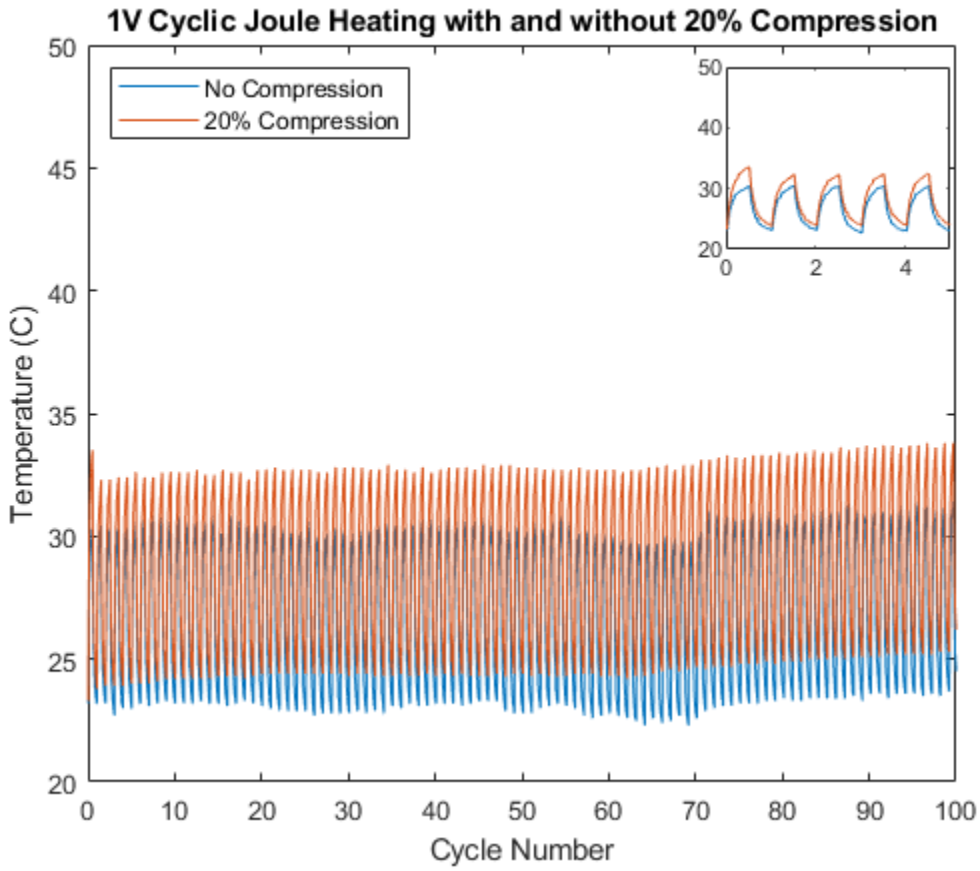

Figure 19: Cyclic joule heating of the strain sensitive sample, C105, at 1 V with and without 20% compression.

For both conditions, with and without compression, the maximum temperature of the sample stays within +/- 2 °C of the maximum temperature of the first cycle. Without compression the temperature of the sample stays around 30 to 31 °C; however, with compression the temperature is increased to 33 to 34 °C.

4.4.4: 1.5 Volts Applied to the Strain Sensitive Sample

The voltage was increased to 1.5 V for cyclic joule heating testing, and the maximum temperature of the sample with and without compression was recorded for 100 cycles of heating and cooling (Figure 20).

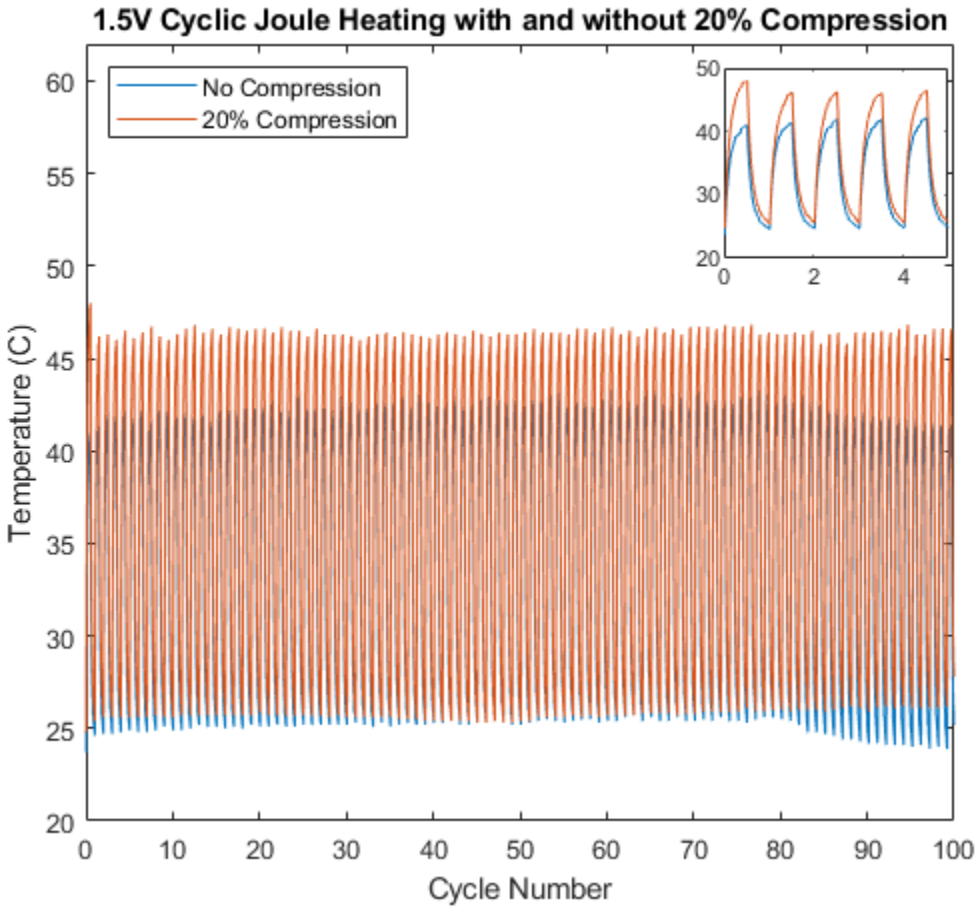

Figure 20: Cyclic joule heating of the strain sensitive sample, C105, at 1.5 V with and without 20% compression.

The difference in maximum temperature reached in each cycle of heating between the compressed sample and uncompressed sample is much larger at 1.5 V applied.

4.5 Thermal Conductivity of the Strain Insensitive Aerogel Recipe

The thermal conductivity of the strain insensitive recipe was measured and compared with commercial cellular and porous materials (Figure 21).

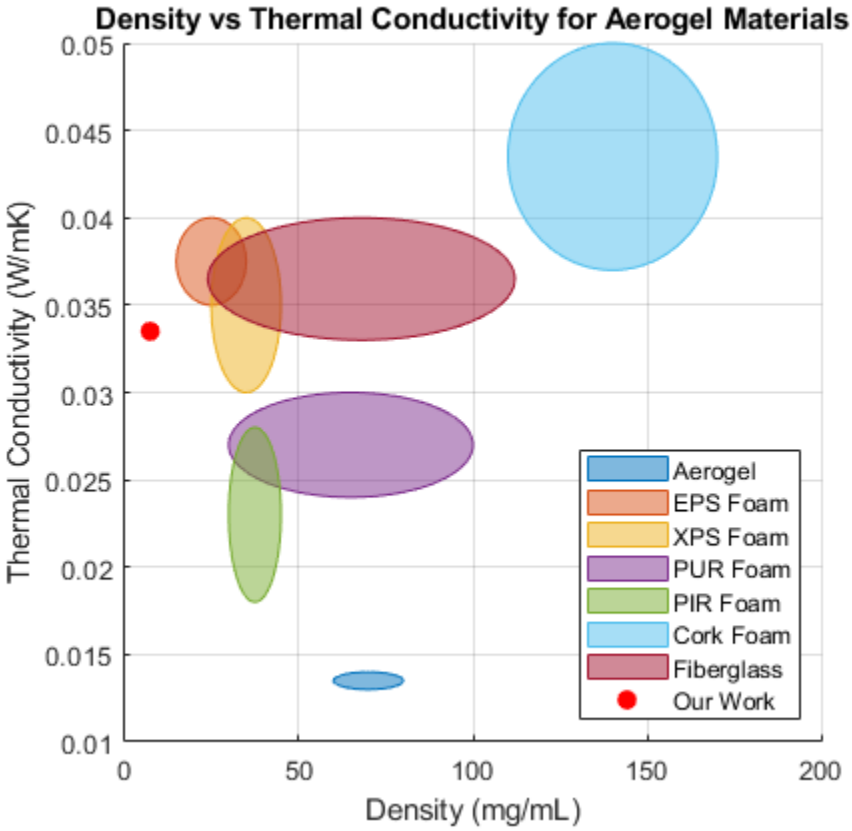

Figure 21: Thermal conductivity and density of recipe C30B (13% cellulose nanofibers, 78% MXene, 9% gelatin, a concentration of 7.5 mg/mL, and no crosslinker) compared with commercial foams and other insulating materials *(11)*

The thermal conductivity of the aerogel recipe was measured as 0.034 W/mK at a density of 7.5 mg/mL. This thermal conductivity is comparable to EPS and XPS commercial foams as well as fiberglass, but it has the added benefit of being much less dense.

5: Discussion and Conclusions

There is interest in the need for personal thermal management in the form of wearable electric heaters for regulating body temperature. Many materials and form factors have been proposed for electric heaters, from two-dimensional materials such as films and fabrics to three dimensional materials, which includes aerogels. Two-dimensional Titanium Carbide (MXene) metal flakes have been used in conductive aerogels due to their excellent electrical properties, and this electrically conductive component was supported with cellulose nanofibers and gelatin at various concentrations between 2.5 to 10 mg/mL to form aerogels. A machine learning model was used to suggest possible recipes to define the design space and these recipes also included the presence or absence of the crosslinker glutaraldehyde.

After forming 131 aerogels of various compositions of MXene, cellulose nanofibers, gelatin, and/or glutaraldehyde, the resistances of these recipes were tested. These compositions of the aerogel recipes were input into a machine learning model along with the output of the measured resistance in order to train an artificial neural network prediction model to suggest aerogel recipes with low resistances. The measured resistance data was subdivided into measurable (200 Ohms or less) and immeasurable (greater than 200 Ohms), and a support vector machine was trained. After active learning loops on the data, a prediction model with an error of 19% was achieved, which can then be used to suggest further recipes with low resistances.

It was experimentally observed that a high MXene loading produced aerogels with low resistances, and recipes with resistances under 100 Ohms were further tested to determine how sensitive their resistances are to changes in applied forces. Of those samples, two recipes were chosen: a strain-insensitive recipe and a strain-sensitive recipe, both with low resistances under 5 Ohms. The Joule heating behavior of both samples were investigated by applying low voltages to

the aerogels and measuring the temperature of the samples over time. Multi-cycle heating tests were also performed with and without 20% compression and it was found that both samples exhibit cyclic temperature stability with no compression. However, when compression was applied, the temperature of the strain-sensitive sample increased by 2 ºC for 1V applied and increased by 4 ºC for 1.5 V applied, while the initial temperature response of the strain-insensitive sample was relatively unchanged under 20% compression compared to the uncompressed temperature behavior.

The thermal conductivity of the strain-insensitive recipe was measured to determine if these electrically conductive aerogels are still suitable for insulation. It was found that the thermal conductivity is comparable to insulating foams and that this thermal conductivity is achieved at a much lower density. More studies may be necessary to explore how aerogel freezing and other formation methods affects the porosity and thus the thermal conductivity.

Bibliography

1. Kistler SS. Coherent Expanded Aerogels and Jellies. Nature. 1931 May;127(3211):741–741.

2. Pierre AC. History of Aerogels. In: Aegerter MA, Leventis N, Koebel MM, editors. Aerogels Handbook [Internet]. New York, NY: Springer; 2011 [cited 2023 Apr 17]. p. 3–18. (Advances in Sol-Gel Derived Materials and Technologies). Available from: https://doi.org/10.1007/978-1-4419-7589-8_1

3. Smirnova I, Gurikov P. Aerogel production: Current status, research directions, and future opportunities. J Supercrit Fluids. 2018 Apr 1;134:228–33.

4. Hu L, He R, Lei H, Fang D. Carbon Aerogel for Insulation Applications: A Review. Int J Thermophys. 2019 Mar 16;40(4):39.

5. Vareda JP, Lamy-Mendes A, Durães L. A reconsideration on the definition of the term aerogel based on current drying trends. Microporous Mesoporous Mater. 2018 Mar 1;258:211–6.

6. Pierre AC, Pajonk GM. Chemistry of Aerogels and Their Applications. Chem Rev. 2002 Nov 1;102(11):4243–66.

7. Maleki H, Durães L, García-González CA, del Gaudio P, Portugal A, Mahmoudi M. Synthesis and biomedical applications of aerogels: Possibilities and challenges. Adv Colloid Interface Sci. 2016 Oct 1;236:1–27.

8. Zou F, Budtova T. Polysaccharide-based aerogels for thermal insulation and superinsulation: An overview. Carbohydr Polym. 2021 Aug 15;266:118130.

9. Dou L, Zhang X, Cheng X, Ma Z, Wang X, Si Y, et al. Hierarchical Cellular Structured Ceramic Nanofibrous Aerogels with Temperature-Invariant Superelasticity for Thermal Insulation. ACS Appl Mater Interfaces. 2019 Aug 14;11(32):29056–64.

10. Al-Homoud DrMS. Performance characteristics and practical applications of common building thermal insulation materials. Build Environ. 2005 Mar 1;40(3):353–66.

11. Hung Anh LD, Pásztory Z. An overview of factors influencing thermal conductivity of building insulation materials. J Build Eng. 2021 Dec 1;44:102604.

12. Hu R, Liu Y, Shin S, Huang S, Ren X, Shu W, et al. Emerging Materials and Strategies for Personal Thermal Management. Adv Energy Mater. 2020;10(17):1903921.

13. Wang Y, Chen L, Cheng H, Wang B, Feng X, Mao Z, et al. Mechanically flexible, waterproof, breathable cellulose/polypyrrole/polyurethane composite aerogels as wearable heaters for personal thermal management. Chem Eng J. 2020 Dec 15;402:126222.

14. Li E, Pan Y, Wang C, Liu C, Shen C, Pan C, et al. Multifunctional and superhydrophobic cellulose composite paper for electromagnetic shielding, hydraulic triboelectric nanogenerator and Joule heating applications. Chem Eng J. 2021 Sep 15;420:129864.

15. Menzel R, Barg S, Miranda M, Anthony DB, Bawaked SM, Mokhtar M, et al. Joule Heating Characteristics of Emulsion-Templated Graphene Aerogels. Adv Funct Mater. 2015;25(1):28–35.

16. Bi L, Yang Z, Chen L, Wu Z, Ye C. Compressible AgNWs/Ti3C2Tx MXene aerogel-based highly sensitive piezoresistive pressure sensor as versatile electronic skins. J Mater Chem A. 2020 Oct 6;8(38):20030–6.

17. Tung TT, Robert C, Castro M, Feller JF, Kim TY, Suh KS. Enhancing the sensitivity of graphene/polyurethane nanocomposite flexible piezo-resistive pressure sensors with magnetite nano-spacers. Carbon. 2016 Nov 1;108:450–60.

18. Gogotsi Y, Anasori B. The Rise of MXenes. ACS Nano. 2019 Aug 27;13(8):8491–4.

19. Li X, Huang Z, Shuck CE, Liang G, Gogotsi Y, Zhi C. MXene chemistry, electrochemistry and energy storage applications. Nat Rev Chem. 2022 Jun;6(6):389–404.

20. Wei C, Zhang Q, Wang Z, Yang W, Lu H, Huang Z, et al. Recent Advances in MXene-Based Aerogels: Fabrication, Performance and Application. Adv Funct Mater. 2023;33(9):2211889.

21. Long LY, Weng YX, Wang YZ. Cellulose Aerogels: Synthesis, Applications, and Prospects. Polymers. 2018 Jun 6;10(6):623.

22. Chen Y, Zhang L, Yang Y, Pang B, Xu W, Duan G, et al. Recent Progress on Nanocellulose Aerogels: Preparation, Modification, Composite Fabrication, Applications. Adv Mater. 2021;33(11):2005569.

23. Wang J, Zhao D, Shang K, Wang YT, Ye DD, Kang AH, et al. Ultrasoft gelatin aerogels for oil contaminant removal. J Mater Chem A. 2016;4(24):9381–9.

24. Guajardo S, Figueroa T, Borges J, Aguayo C, Fernández K. Graphene oxide-gelatin aerogels as wound dressings with improved hemostatic properties. Mater Today Chem. 2021 Jun 1;20:100418.

25. Yang M, Yuan Y, Li Y, Sun X, Wang S, Liang L, et al. Anisotropic Electromagnetic Absorption of Aligned Ti3C2Tx MXene/Gelatin Nanocomposite Aerogels. ACS Appl Mater Interfaces. 2020 Jul 22;12(29):33128–38.

26. Bi Q, Goodman KE, Kaminsky J, Lessler J. What is Machine Learning? A Primer for the Epidemiologist. Am J Epidemiol. 2019 Dec 31;188(12):2222–39.

27. Fradkov AL. Early History of Machine Learning. IFAC-Pap. 2020 Jan 1;53(2):1385–90.

28. Wei J, Chu X, Sun XY, Xu K, Deng HX, Chen J, et al. Machine learning in materials science. InfoMat. 2019;1(3):338–58.

29. Saito T. Self-aligned integration of native cellulose nanofibrils towards producing diverse bulk materials. Soft Matter. 2011 Aug 23;7:8804–9.

30. Yang H, Li J, Lim KZ, Pan C, Van Truong T, Wang Q, et al. Automatic strain sensor design via active learning and data augmentation for soft machines. Nat Mach Intell. 2022 Jan;4(1):84–94.

31. Noble WS. What is a support vector machine? Nat Biotechnol. 2006 Dec;24(12):1565–7.

32. Kim SC, Oyakhire ST, Athanitis C, Wang J, Zhang Z, Zhang W, et al. Data-driven electrolyte design for lithium metal anodes. Proc Natl Acad Sci. 2023 Mar 7;120(10):e2214357120.

33. Bologna G. A Rule Extraction Technique Applied to Ensembles of Neural Networks, Random Forests, and Gradient-Boosted Trees. Algorithms. 2021 Dec;14(12):339.

34. Rodríguez-Pérez R, Bajorath J. Interpretation of machine learning models using shapley values: application to compound potency and multi-target activity predictions. J Comput Aided Mol Des. 2020 Oct 1;34(10):1013–26.